10040–10058 *Nucleic Acids Research, 2019, Vol. 47, No. 19* *Published online 20 August 2019*
doi: 10.1093/nar/gkz722

Post-transcriptional negative feedback regulation of proteostasis through the Dis3 ribonuclease and its disruption by polyQ-expanded Huntingtin

Ka-Yiu Edwin Kong*, Ting-Ngai Felix Hung, Pui-Hei Marcus Man, Tin-Ning Wong, Tao Cheng and Dong-Yan Jin*

School of Biomedical Sciences, The University of Hong Kong, Hong Kong

Received March 05, 2019; Revised August 05, 2019; Editorial Decision August 06, 2019; Accepted August 08, 2019

ABSTRACT

When proteostasis is disrupted by stresses such as heat shock, the heat stress response will be stimulated, leading to up-regulation of molecular chaperones by transcriptional activation and mRNA stabilization for restoring proteostasis. Although the mechanisms for their transcriptional activation have been clearly defined, how chaperone mRNAs are stabilized remains largely unknown. Starting by exploring the coupling between the apparently unrelated RNA degradation and protein quality control (PQC) systems, we show that the Dis3 ribonuclease, catalytic subunit of the RNA exosome required for RNA degradation, suppresses PQC activity in unstressed cells by degrading mRNAs encoding the Hsp70 cofactors Sis1, Ydj1 and Fes1, as well as some other chaperones or PQC factors, thereby limiting their protein expression. Dis3 is stabilized through its binding to Sis1 and the Hsp70s Ssa1/2. Upon heat stress, loss of Sis1 and Ssa1/2 availability triggers Dis3 ubiquitination and degradation, leading to stabilization of those chaperone mRNAs originally targeted by Dis3. We further demonstrate that polyQ-expanded huntingtin delays Dis3 degradation during heat stress and thus hinders chaperone mRNA stabilization. Our findings not only reveal a post-transcriptional negative feedback loop for maintaining proteostasis, but also uncover a mechanism that contributes to the impaired heat stress response in Huntington's disease.

INTRODUCTION

Eukaryotic cells have evolved the highly sophisticated RNA degradation and protein quality control (PQC) systems that constantly monitor the emergence of aberrant RNAs and misfolded proteins respectively, and then target them to degradation or sequestration for preventing these potentially harmful species from affecting cell physiology. In yeast, RNA degradation is performed by an elaborate network of ribonucleases, including Xrn1 and the multisubunit exosome complex that have different substrate specificities. Xrn1 is a cytoplasmic 5′-3′ exoribonuclease that functions in the turnover of mRNAs (1) as well as in nonsense-mediated RNA decay (NMD) (2). The core exosome complex, which can be found in both the nucleus and cytoplasm, contains nine structural subunits such as Rrp41 and the only catalytic subunit Dis3 (3), which possesses both 3′-5′ exoribonuclease (4) and endoribonuclease (5) activities. Most aberrant RNAs, such as unspliced pre-mRNAs (6) and hypomodified tRNAs (7) in the nucleus, as well as the RNA substrates of the cytoplasmic NMD and nonstop decay (NSD) pathways (8), are susceptible to Dis3-mediated degradation. In addition, Dis3 is involved in the turnover of normal mRNAs as well as in the accelerated degradation of mRNAs containing the destabilizing AU-rich elements (AREs) (1,9). The nuclear exosome associates with an additional catalytic subunit Rrp6, which is a 3′-5′ exoribonuclease that removes pre-mRNAs that cannot be spliced (10), cryptic unstable transcripts (11) and some other nuclear aberrant RNAs.

PQC requires the action of multiple molecular chaperones and other factors including E3 ligases and the proteasome. Most cytosolic misfolded proteins are degraded by the PQC system, which involves their recognition by Hsp70s such as Ssa1, then nuclear import by the Hsp40 Sis1, and finally degradation by the nuclear proteasome (12), with the cytosolic E3 ligase Ubr1 and the nuclear E3 ligase San1 acting in parallel to ubiquitinate the misfolded proteins (13–15). Their degradation also requires the Hsp40 Ydj1 and the Hsp70 nucleotide exchange factor Fes1, which act by stimulating Hsp70 activity (16) and by promoting misfolded protein release from Hsp70 (17), respectively. If the abundance of misfolded proteins overwhelms this degradation pathway, the excess misfolded proteins will be deposited into

*To whom correspondence should be addressed. Tel: +852 39176812; Fax: +852 28551254; Email: ewedwin@hku.hk
Correspondence may also be addressed to Dong-Yan Jin. Tel: +852 39179491; Fax: +852 28551254; Email: dyjin@hku.hk

the intra-nuclear quality control (INQ), the cytosolic quality control (CytoQ), and/or the insoluble protein deposit (IPOD) compartments depending on their solubility and ubiquitination status (18,19). The formation of INQ is dependent on the small heat shock protein (sHSP) Btn2, while that of CytoQ requires another sHSP Hsp42 (19,20). This active sequestration of misfolded proteins not only serves to prevent their aberrant interaction with important cellular factors, but may also enhance their subsequent removal once the degradation machinery is available.

During normal growth condition, the capacity of the PQC system is sufficient to handle misfolded proteins and maintain protein homeostasis (proteostasis). However, when the cells encounter heat stress or other proteotoxic situations, the production of a huge amount of misfolded proteins exceeding PQC capacity can lead to proteostasis imbalance, which will then elicit the cellular heat stress response, resulting in the rapid up-regulation of molecular chaperones and PQC factors that can restore proteostasis. In the classical heat stress response pathway, the Hsf1 transcription factor that is normally inactivated due to complex formation with the Hsp70 and Hsp90 chaperones is promptly converted into a potent transcription activator upon heat stress as a result of the titration of Hsp70 and Hsp90 away from Hsf1 by the massive amount of misfolded proteins (21,22), and then stimulates transcription of genes encoding molecular chaperones and PQC factors. In addition to transcriptional activation, stabilization of some of their corresponding mRNAs by unknown mechanisms also contributes to their increased expression during heat stress (23–26). Interestingly, it has been reported that polyQ-expanded huntingtin can suppress the heat stress response at least partially by lowering Hsf1 expression (27), which may lead to the gradual decline of proteostasis capacity in Huntington's disease. Conversely, pharmacological activation of the heat stress response can alleviate polyQ-expanded huntingtin toxicity (28–30). Therefore, further study of how the heat stress response is activated and maintained will certainly enhance our understanding on the regulation of proteostasis, and may reveal novel strategies to combat Huntington's or other neurodegenerative diseases by stimulating the heat stress response.

We began this study as we were curious about whether there is any coupling between the seemingly unrelated RNA degradation and PQC systems. This hypothesis was based on the fact that some aberrant RNAs (substrates for RNA degradation), such as unspliced pre-mRNAs and nonstop RNAs, could be translated into non-native proteins that were prone to misfolding (substrates for PQC), which suggested the necessity for the up-regulation of PQC activity upon malfunctions of the RNA degradation pathway in order to prepare for the handling of the upcoming amount of misfolded proteins. Starting by testing this hypothesis, we eventually identified a post-transcriptional negative feedback loop that regulates PQC activity through the RNA degradation factor Dis3. We further showed that this post-transcriptional pathway is required for the stabilization of a subset of chaperone mRNAs during heat stress, and that its disruption by polyQ-expanded huntingtin contributes to the resultant heat stress response impairment, providing completely new insights into the disease mechanisms and pharmacological treatment of Huntington's and other neurodegenerative diseases.

MATERIALS AND METHODS

Yeast media and growth conditions

Yeast cells were routinely cultured at 30°C in YPD medium (1% yeast extract, 2% peptone, 2% glucose) for cells without plasmids, or in synthetic complete (SC) medium lacking the appropriate amino acids but containing 2% glucose (Glu) as the only carbon source for plasmid-containing cells. Some 2% agar was also included for agar plates. If needed, DOX (10μg/ml) was added for the depletion of Dis3 or Sis1. Cell harvesting was performed when the OD_{600} of the yeast cultures reached ∼0.5–0.8. All yeast transformations were achieved using the standard lithium acetate method (31).

For galactose (Gal) induction of protein expression, 1:500 of overnight yeast cultures in SC-2%Glu was added to SC-2%Gal medium and then incubated for 18 h until OD_{600} ∼0.5–0.8. For 39°C heat shock treatment, yeast cells were first spun down and then resuspended in 10% volume of the original culturing medium, followed by placing the resultant 10-fold concentrated yeast cultures into a 39°C water bath for the indicated amount of time. For proteasome inhibition, MG132 (80 μM) was added to cells lacking the multidrug exporter Pdr5.

Yeast strain constructions

The yeast strains used in this work are listed in Supplementary Table S1. While most strains were derived from BY4742, the strains that were related to Sis1 depletion and *RRP6* or *XRN1* deletions corresponded to the BY4741 background. Other than those obtained from the Butler's laboratory or commercially available from Dharmacon, yeast strains were constructed using the homologous recombination techniques as described below.

To generate yeast cells expressing C-terminal Flag-tagged endogenous Sis1 or Ssa1 without affecting the 3′-UTR of their corresponding mRNAs, a self-designed two-step homologous recombination method was used. First, the 500bp 3′-UTR sequences plus the stop codon of the *SIS1* or *SSA1* genes was replaced by the *mCHERRY*::*HphMX6* cassette, which was PCR-amplified from pFA6a-mCherry-hphMX6 using primers SIS1_F_mChe_hph and SIS1_R_mChe_hph or SSA1_F_mChe_hph and SSA1_R_mChe_hph. Successful recombinants were selected on YPD agar plates containing hygromycin (300 μg/ml) (Invivogen ant-hg-1) and then further confirmed by PCR. Deletion of the 3′-UTR sequences in this first round of recombination allowed the insertion of the *FLAG*::*SIS1-WT-3′UTR*::*HIS3* or *FLAG*::*SSA1-WT-3′UTR*::*HIS3* cassettes during the second recombination step, exactly replacing the *mCHERRY*::*HphMX6* sequences. These two *FLAG*::*HIS3* cassettes were PCR-amplified from the pFA6a-Flag-[Sis1-WT-3′UTR]-His3MX6 or pFA6a-Flag-[Ssa1-WT-3′UTR]-His3MX6 plasmids, which were derived from pFA6a-13Myc-His3MX6 by replacing the original 13Myc-Adh1–3′UTR regions with the Flag-Sis1-WT-3′UTR or Flag-Ssa1-WT-3′UTR sequences via the BamHI and BglII restriction sites. The

primer pairs SIS1_F_Flag_HIS and SIS1_R_Flag_HIS or SSA1_F_Flag_HIS and SSA1_R_Flag_HIS were used for the PCR. Selection by SC agar plates lacking histidine followed by PCR and Western blot verification were used to obtain the successful clones, which expressed mRNAs that encoded the Sis1-Flag or Ssa1-Flag proteins and contained the WT *SIS1* or *SSA1* 3′-UTRs. The same strategy was applied to construct yeast strains expressing *SIS1-FLAG* mRNA with ARE mutation, except that pFA6a-Flag-[Sis1-AREmut-3′UTR]-His3MX6 was used as template to produce the second homologous recombination cassette. The pFA6a-Flag-[Sis1-AREmut-3′UTR]-His3MX6 plasmid was generated from pFA6a-Flag-[Sis1-WT-3′UTR]-His3MX6 by mutating the 'ATTTA' ARE motifs to 'AGGGA' using the Q5® Site-Directed Mutagenesis Kit (NEB E0554S) according to manufacturer's instructions, with the sequences of the mutated region and its surroundings being subsequently confirmed by DNA sequencing.

The CMV-tTA Dis3-GFP strain was constructed from CMV-tTA using the standard one-step homologous recombination procedures that involved the integration of the *yEGFP*::*KanMX* fragment just downstream of the *DIS3* coding sequences. This integration cassette was PCR-amplified from the pKT127 plasmid using the primers Dis3_F_GFP_tag and Dis3_R_GFP_tag. The further deletion of *PDR5* in the CMV-tTA Dis3-GFP strain was achieved by the recombination of the *HphMX6* cassette generated from the pFA6a-mCherry-hphMX6 template using the primers PDR5_DEL_F_hph and PDR5_DEL_R_hph without amplifying the mCherry sequences. Similar to the CMV-tTA Dis3-GFP strain, GFP-tagging of Dis3 in the commercially-available TetOff-Sis1 cells was made by the insertion of the *yEGFP*::*SpHIS5* fragment that was obtained using pKT128 as template and Dis3_F_GFP_tag plus Dis3_R_GFP_tag as primers. The single or double deletions of *SSA1* and *SSA2* in CMV-tTA Dis3-GFP cells were introduced by replacing the entire coding sequences with the *HIS3* (for *SSA1*) or *HphMX6* (for *SSA2*) cassettes. The primers SSA1_DEL_F_HIS and SSA1_DEL_R_HIS were used to synthesize the *HIS3* cassette from the pFA6a-His3MX6 template, while SSA2_DEL_F_hph and SSA2_DEL_R_hph were employed to amplify the *HphMX6* cassette from pFA6a-mCherry-hphMX6. Epitope tagging of Sis1 by Myc or Ssa1/2 by Flag were done in the CMV-tTA Dis3-GFP, CMV-tTA Dis3-GFP *pdr5*Δ and CMV-tTA backgrounds through the integration of the *MYC*::*HIS3* or *FLAG*::*HIS3* fragments just downstream of the coding sequences. For the *MYC*::*HIS3* cassette, pFA6a-13Myc-His3MX6 was employed as the template for PCR amplification by the SIS1_F_MYC_HIS and SIS1_R_MYC_HIS primers; while for the *FLAG*::*HIS3* cassette, the template used was pFA6a-Flag-[Hsp82-WT-3′UTR]-His3MX6 and the primers used were SSA1_F_FLAG_HIS and SSA1_R_FLAG_HIS or SSA2_F_FLAG_HIS and SSA2_R_FLAG_HIS.

CMV-tTA Dis3-Myc and CMV-tTA Dis3-Flag were made by transforming the *MYC*::*HIS3* and *FLAG*::*HIS3* cassettes respectively into CMV-tTA. These cassettes were obtained by PCR amplification using the pFA6a-13Myc-His3MX6 and pFA6a-Flag-[Hsp82-WT-3′UTR]-His3MX6 templates respectively with the DIS3_F_tag_HIS and DIS3_R_tag_HIS primers. The TetOff-Dis3-Myc strain was constructed similarly from TetOff-Dis3 using the *MYC*::*HIS3* cassette.

In all cases, the yeast cells with the desired genetic modifications were first selected on YPD agar plates with addition of the appropriate antibiotics or SC agar plates lacking the appropriate amino acids. Candidate clones were then subjected to further verification by PCR, and for epitope tagging, also by Western blot analyses. The sequences of all primers used in yeast strain constructions can be found in Supplementary Table S3.

Plasmid constructions

All plasmids used in this work are listed in Supplementary Table S2. The pRS413Gal1-CG* plasmid was cloned by four steps. First, the *GFP* sequence PCR-amplified from pKT127 was inserted into pRS413Gal1 through the SpeI and XhoI restriction sites to produce pRS413Gal1-GFP, and then the *PRC1* gene (encoding carboxypeptidase Y, or CPY) without stop codon was amplified from yeast genomic DNA and cloned just upstream of the *GFP* sequence via the SpeI sites at both ends, forming pRS413Gal1-CPY-GFP. After that, the previously described mutation of the 255th codon of *PRC1* from 'GGG' to 'AGG' (from glycine to arginine at the protein level) (32), as well as the removal of the ER signal sequence (33), were done sequentially by the Q5® Site-Directed Mutagenesis Kit (NEB E0554S), generating pRS413Gal1-CPY*-GFP (referred to as pRS413Gal1-CG* in this paper). To construct pRS413Gal1-WT-Luc-GFP, the WT-Luc gene without stop codon amplified from pGL3-Basic was inserted into pRS413Gal1-GFP using SpeI sites at both ends. Site-directed mutagenesis of both the 188th codon from 'AGG' to 'CAG' and the 261st codon from 'CGA' to 'CAA' (both resulted in the mutation of arginine to glutamine at the protein level) (34) resulted in the formation of pRS413Gal1-DM-Luc-GFP.

For plasmids expressing Dis3 with or without mutations of its catalytic sites, pRS415-Dis3(WT) was first constructed by introducing the entire *DIS3* gene plus 269bp of upstream promoter sequence and 290bp of downstream terminator sequence into the pRS415 backbone using the SacII and SpeI sites. Mutations of its exoribonuclease [G1651A(DNA) D551N(protein)] and endoribonuclease [G511A(DNA) D171N(protein)] sites by the mutagenesis kit led to the generation of pRS415-Dis3(exo$^-$), pRS415-Dis3(endo$^-$), and pRS415-Dis3(exo$^-$endo$^-$). Addition of the Flag-tag sequence just downstream of *DIS3* using the mutagenesis kit produced pRS415-Dis3-Flag(WT), pRS415-Dis3-Flag(exo$^-$), pRS415-Dis3-Flag(endo$^-$) and pRS415-Dis3-Flag(exo$^-$endo$^-$).

To generate the galactose promoter-driven luciferase gene attached to the *SIS1* terminator with or without ARE mutation, the luciferase sequence PCR-amplified from pRS413Gal1-WT-Luc-GFP was first cloned into pRS415Gal1 using the BamHI and HindIII sites, and then the WT or AREmut *SIS1* terminator sequences PCR-amplified from pFA6a-Flag-[Sis1-WT-3′UTR]-His3MX6 or pFA6a-Flag-[Sis1-AREmut-3′UTR]-His3MX6 respec-

tively were inserted just downstream of the luciferase gene via HindIII and XhoI.

To clone the expression constructs for HA-tagged Sis1, Ssa1, and Dis3, their coding sequences were PCR-amplified from genomic DNA with the reverse primers containing an incorporated HA-tag sequence, and then inserted into pRS415Gal1 using the restriction sites SpeI and PstI (for Sis1 and Dis3) or SpeI and HindIII (for Ssa1). For the construction of pRS413Gal1-Myc-mCherry-Htt25Q and pRS413Gal1-Myc-mCherry-Htt96Q, the *MYC-mCHERRY* fragment without stop codon was synthesized from the pFA6a-mCherry-hphMX6 template using a forward primer containing an intrinsic Myc-tag sequence. This fragment was then ligated into pRS413Gal1 via the SpeI and BamHI sites to form pRS413Gal1-Myc-mCherry. After that, insertion of the Htt25Q and Htt96Q sequences amplified from Tag2B-Htt25Q and Tag2B-Htt96Q respectively resulted in the production of pRS413Gal1-Myc-mCherry-Htt25Q and pRS413Gal1-Myc-mCherry-Htt96Q. The restriction sites involved were BamHI(vector)-BglII (insert) and XhoI. A similar strategy was employed to synthesize pRS425Gal1-Myc-mCherry-Htt25Q and pRS425Gal1-Myc-mCherry-Htt96Q.

Western blotting

Around 5–8 OD of yeast cells were lysed by the previously described alkaline lysis method (35). First, cells were resuspended in 450μl of lysis buffer (0.25 M NaOH and 1% β-mercaptoethanol) and incubated for 10 min on ice. After that, 50 μl of trichloroacetic acid (TCA; final concentration 10%) was added and incubated for another 10 min to allow precipitation of both soluble and insoluble proteins. Then, the protein pellets obtained after centrifugation at maximum speed for 5 min were washed once with 1 ml of 100% ethanol, resuspended in 200 μl of solubilization buffer (8 M urea and 10 mM β-mercaptoethanol), and incubated at 4°C for 1 h for protein solubilization. Finally, 100 μl of the cell lysates were mixed with 25 μl of 5X standard protein sample buffer to obtain the final protein samples, and 10 μl of each sample was then subjected to SDS-PAGE and immunoblotting analyses. The antibodies used were: Anti-GFP (Santa Cruz sc-9996; 1:1000); Anti-PGK1 (Novex 459250; 1:5000); Anti-FLAG (Sigma-Aldrich F3165; 1:5000); Anti-HA (Santa Cruz sc-7392; 1:1000); Anti-MYC (Santa Cruz sc-40; 1:1000); Anti-Ubiquitin (Santa Cruz sc-8017; 1:1000). The ImageJ software developed by NIH was applied to quantify all western blot data. Band intensity of the protein of interest was normalized to that of the loading control PGK1.

Cycloheximide (CHX) chase assay

CHX (0.5mg/ml) was added directly to yeast cultures at OD_{600} ∼0.5–0.8 to stop protein synthesis, and then ∼5–8 OD (10 ml) cells were harvested at each time point. Relative expression levels of the reporter proteins at different time points were then analyzed by western blot as described above.

Luciferase (Luc) activity measurement

Luc activity was measured using the Dual-Luciferase® Reporter Assay System (Promega E1960). Yeast cultures at OD_{600} ∼0.5–0.8 were first normalized according to their cell densities, and then cell lysis was performed by mixing 15 μl of yeast cultures with 100 μl of 1× passive lysis buffer. Working very quickly, 15 μl of the resultant cell lysates was transferred into a 96-well luminometry plate, followed by the immediate addition of 50μl of luciferase assay buffer II with substrate, and the measurement of Luc activity by a luminometer.

Quantitative reverse transcription PCR (RT-qPCR)

Total RNA in ∼5–8 OD of yeast cells was extracted using the hot phenol method. Cell pellets were first resuspended in 400 μl of AE buffer (50 mM NaOAc pH 5.2, 10 mM EDTA) plus 40 μl of 10% SDS and 400 μl of acidic phenol:chloroform (pH ∼4.5) pre-warmed to 65°C, and then incubated in a 65°C water bath for 10 min. After phase separation by centrifugation for 10 min at maximum speed, the lower organic layer was discarded, and the upper aqueous fraction was washed twice with an equal volume of acidic phenol:chloroform and then once with chloroform. Ethanol precipitation was then used to obtain the RNA pellets, which were subsequently de-salted by 70% ethanol, air-dried for 10 min, and finally resuspended in DEPC-treated water. Removal of contaminating genomic DNA followed by reverse transcription was done by the PrimeScript™ RT Reagent Kit with gDNA Eraser (TaKaRa RR047A) using 1μg of total RNA. Relative expression levels of the mRNAs of interest, and also that of the control RNAs *PGK1* (for experiments involving Dis3 depletion) or *SCR1* (for experiments not involving Dis3 depletion), were determined by qPCR using the SYBR® Premix Ex Taq™ (Tli RNaseH Plus) reagent (TaKaRa RR420A) according to manufacturer's instructions. All samples were analyzed in triplicates. The relative standard curve method was used to determine the levels of the target mRNAs relative to that of the controls *PGK1* or *SCR1*. Data analyses were done by the StepOne software provided by Applied Biosystems. The primers used for qPCR can be found in Supplementary Table S3.

RNA sequencing

Total RNA was first extracted by the hot phenol method as described above. Library preparation and Illumina sequencing (pair-end sequencing of 151 bp) were done at the Centre for Genomic Sciences of The University of Hong Kong. The cDNA libraries were prepared by the KAPA Stranded mRNA-Seq Kit (Kapa Biosystems KK8421) using 1μg of total RNA as starting material according to manufacturer's protocol. In brief, poly-A containing mRNA was collected by using poly-T oligo-attached magnetic beads. The purified mRNA was fragmented to 200–300 bp by incubating at 94°C for 6 min in the presence of magnesium ions. The fragmented mRNA was then applied as template to synthesize the first-strand cDNA by using random hexamer-primer and reverse transcriptase. In the second strand cDNA synthesis, the mRNA template was re-

moved and a replacement strand was generated to form the blunt-end double-stranded (ds) cDNA. The ds-cDNA underwent 3′-adenylation and indexed adaptor ligation. The adaptor–ligated libraries were enriched by 10 cycles of PCR. The libraries were then denatured and diluted to optimal concentration. Illumina NovaSeq 6000 was used for pair-end 151bp sequencing. Sequencing reads were first filtered for adapter sequence and low quality sequence followed by retaining only reads with read length $\geq$ 40bp. Subsequently, sequencing reads were filtered for rRNA sequence and remaining reads were used for downstream analysis. Reads were mapped to the reference yeast genome R64-1-1 (downloaded from iGenome) using STAR (default parameters) with the following exception: [twopassMode: Basic]. Differential expression analysis was done using EBSeq.

Chromatin immunoprecipitation (ChIP)

Around 5–8 OD of yeast cells were first crosslinked by 1% formaldehyde for 15 min, and then lysed in 1 ml of FA lysis buffer (50 mM HEPES–KOH pH 7.5, 140 mM NaCl, 1 mM EDTA, 1% Triton X-100, 0.1% Na-deoxycholate, and protease inhibitors) by vigorous vortexing for 10 min in the presence of glass beads. Cell lysates were then sonicated using a Sonics Vibra-cell sonicator for a total of 5 min, with 9 s rest after every 9 s of sonication, followed by the removal of cell debris by centrifugation. Immunoprecipitation of Rpb3 and its associated chromatin fragments within 200 μl of the sonicated cell lysates was performed by the addition of 40 μl of Dynabeads™ M-280 Sheep Anti-Mouse IgG (Invitrogen 11202D) being pre-incubated with 0.5 μl of Anti-Rpb3 antibody (Neoclone W0012). After 2 h of immunoprecipitation at 4°C, the beads were washed sequentially with FA lysis buffer, wash buffer II (50 mM HEPES–KOH pH 7.5, 500 mM NaCl, 1 mM EDTA, 1% Triton X-100, 0.1% Na deoxycholate), wash buffer III (10 mM Tris–HCl pH 8.0, 250 mM LiCl, 1 mM EDTA, 0.5% NP-40, 0.5% Na deoxycholate), and finally TE buffer (10 mM Tris–HCl pH 8.0, 1 mM EDTA). Then, the chromatin fragments still bound to the washed beads were eluted and their crosslinks with Rpb3 were reversed in 250 μl of elution buffer (10 mM Tris–HCl pH 8.0, 1 mM EDTA, 0.67% SDS) by overnight incubation at 65°C. Input lysates (50 μl) were also processed alongside the immunoprecipitated samples for crosslink reversal. After that, the DNA fragments within the input and immunoprecipitated samples were purified by phenol-chloroform extraction and ethanol precipitation. Finally, the relative amount of the interested chromatin fragments and a noncoding region within chromosome V (ChrV) in both the input and immunoprecipitated samples was quantified by qPCR as described above. Rpb3 occupancies were then calculated by the following formula: $\{2^{Ct(IP:ChrV) - Ct(IP:Rpb3)}/2^{Ct(Input:ChrV) - Ct(Input:Rpb3)}\}$. All primers used are listed in Supplementary Table S3.

Analyses of mRNA stability

SIS1 mRNA stability was determined from the degradation kinetics of excess *SIS1* mRNA during 30°C recovery after an acute heat shock at 39°C for 20 min. Stability of the luciferase mRNA containing the *SIS1* 3′-UTR with or without ARE mutation was measured after its transcriptional shut off with 4% glucose, while that of the *SIS1*, *YDJ1*, and *FES1* mRNAs during heat shock was monitored after addition of the transcriptional inhibitor thiolutin (3 μg/ml). Around 5–8 OD cells were harvested at the indicated time points for the subsequent analyses of their mRNA levels by RT-qPCR as described above.

Co-immunoprecipitation (CoIP)

Around 10–16 OD of yeast cells were lysed in 300μl of IP buffer (50 mM Tris–HCl pH 7.5, 100 mM NaCl, 0.5 mM EDTA, 1% NP-40, 0.1% Na-deoxycholate and protease inhibitors, with addition of 10 mM *N*-ethylmaleimide for ubiquitination experiments) and glass beads by vortexing at 4°C for 3 min, with 30 s rest after each 30 s of vortexing. After centrifugation, 200 μl of supernatants were used for the immunoprecipitation of Dis3-GFP by 0.2 μl of Anti-GFP antibody (Abcam ab290) pre-attached to 40 μl of Dynabeads™ M-280 Sheep Anti-Rabbit IgG (Invitrogen 11204D). After incubation at 4°C for 2 h, the beads were washed twice with 1 ml of IP buffer, and then resuspended in 100 μl of IP buffer and 25 μl of 5× standard protein sample buffer. Thereafter, the immunoprecipitated proteins were eluted by boiling for 15 min, followed by western blotting to detect the presence of Dis3-GFP, and also its ubiquitin chain or interaction partners Sis1-Myc and Ssa1/2-Flag.

Confocal microscopy

Confocal imaging was performed using the Carl Zeiss LSM 700 inverted fluorescence microscope. Yeast cells being crosslinked by 1% formaldehyde for 10 min were used for imaging. The ZEN 2010 software provided by Zeiss was employed for image processing.

Solubility assay

Yeast cells were lysed by the same method as that used for CoIP, except that 250 μl of Triton lysis buffer (100 mM HEPES–KOH pH 7.5, 300 mM NaCl, 1% Triton X-100 and protease inhibitors) was used instead of IP buffer. The resultant cell lysate was centrifuged at 1500 × g for 5 min, and the supernatant (220 μl) was then collected as the total protein fraction (T). After that, half (110 μl) of the total fraction was subjected to centrifugation at maximum speed for 10 min for the separation of soluble and insoluble proteins. The supernatant was regarded as the soluble fraction (S), while the pellet was further resuspended in the initial volume (110 μl) of Triton lysis buffer, forming the insoluble pellet fraction (P). All three fractions were subsequently analyzed by western blotting.

Statistical analyses

The number of biological replicates and whether the error bars represent the SD or SEM are indicated in the figure legends. Two-tailed Student's *t*-test was used to determine whether any observed differences were statistically significant, which was defined as $P < 0.05$. In all figures, N.S.:

non-significant; *$P < 0.05$; **$P < 0.01$. Standard Pearson's chi-squared test was applied to test for the enrichment of the 'AUUUA' motif in Dis3 mRNA substrates.

RESULTS

Dis3 is a negative regulator of PQC activity and protein folding capacity

To explore the possible coupling between the RNA degradation and PQC systems, we tested whether inactivation of the RNA degradation pathway may affect PQC activity. The degradation kinetics of the terminally misfolded protein CPY*-GFP (abbreviated as CG* thereafter) (12,16) was analyzed in cells with or without doxycycline (DOX)-mediated Dis3 depletion via a tetracycline-off (TetOff) promoter. Interestingly, the degradation of CG* was significantly accelerated upon Dis3 depletion (Figure 1A and B), indicating that Dis3 or the RNA degradation system negatively regulated misfolded protein degradation. In control cells, ∼40% of the original CG* protein was still present 2 h after CHX addition; while in Dis3-depleted cells, only <30% of CG* remained even at the 1 h time point (Figure 1B). Confocal microscopy showed that CG* readily formed detectable aggregates, with ∼50% of cells without Dis3 depletion containing such aggregates mostly in the form of a single large cytoplasmic inclusion (Supplementary Figure S1). Consistent with a negative regulatory role of Dis3 in PQC, depletion of Dis3 moderately alleviated CG* aggregation, with only 25% of cells having CG* aggregates which were often much smaller than that observed in control cells (Supplementary Figure S1).

In addition, we also examined the overall protein folding capacity in cells with or without Dis3 depletion using a well-characterized firefly luciferase-based system (34). This system involved the use of a destabilized mutant of firefly luciferase (DM-Luc), which required frequent interaction with molecular chaperones in order to maintain its properly-folded enzymatically-active state, and could therefore serve as a reporter for chaperone availability and overall protein folding capacity. Depletion of Dis3 had no significant effect on WT-Luc-GFP activity (Figure 1C), which was expected given that WT-Luc-GFP should be constitutively folded. On the other hand, DM-Luc-GFP activity increased more than 2-fold (Figure 1D) despite that its protein expression level was not significantly altered (Figure 1E), suggesting a gain in chaperone availability and protein folding capacity.

In order to address whether the suppression of PQC activity and protein folding capacity is dependent on Dis3 alone or the entire core exosome complex, we depleted the exosome structural subunit Rrp41 by the same method and observed for any changes in CG* degradation and DM-Luc-GFP folding. The accelerated CG* degradation (Supplementary Figure S2A) and enhanced DM-Luc-GFP folding (Supplementary Figure S2B and C) upon Rrp41 depletion conveyed the involvement of the entire core exosome complex. In contrast, depletion of the unrelated essential proteins Sec61 or Prp42 did not lead to similar effects (Supplementary Figure S2D–G), excluding the possibility that increased PQC activity and protein folding capacity were the general consequences of the depletion of essential proteins.

We then set out to determine whether PQC may also be regulated by other members of the RNA degradation system. To this end, we analyzed CG* degradation and DM-Luc-GFP folding in cells lacking the nuclear exosome-associated 3′-5′ exoribonuclease Rrp6 or the cytoplasmic 5′-3′ exoribonuclease Xrn1. Unlike *DIS3*, deletion of *RRP6* or *XRN1* only marginally affected the degradation kinetics of CG* (Supplementary Figure S3A). While CG* degradation was barely faster in *rrp6*Δ cells, its degradation was slightly impeded in *xrn1*Δ cells (Supplementary Figure S3A). In addition, deletion of *XRN1* had no significant impact on both WT-Luc-GFP and DM-Luc-GFP activities (Supplementary Figure S3B and C). Although DM-Luc-GFP activity showed some decrease in *rrp6*Δ cells (Supplementary Figure S3C), it was probably not due to reduced folding efficiency but rather lower expression level of DM-Luc-GFP, as both WT-Luc-GFP activity (Supplementary Figure S3B) and WT/DM-Luc-GFP protein levels (Supplementary Figure S3D) also decreased similarly. These results implied that the RNA degradation pathways mediated by Rrp6 and Xrn1 had no significant effect on PQC regulation. Therefore, we concluded that the RNA degradation system suppressed PQC activity and protein folding capacity primarily through the action of Dis3 or the core exosome.

Loss of both 3′-5′ exoribonuclease and endoribonuclease activities of Dis3 is required to boost PQC activity and protein folding capacity

Dis3 possesses both 3′-5′ exoribonuclease (4) and endoribonuclease (5) activities to process or degrade its RNA substrates. We constructed plasmids that could express wild-type Dis3 (Dis3-WT) or its mutants defective in 3′-5′ exoribonuclease activity (D551N; Dis3-exo$^-$), endoribonuclease activity (D171N; Dis3-endo$^-$), or both (D551N D171N; Dis3-exo$^-$endo$^-$), and examined how their expression affected CG* degradation and DM-Luc-GFP folding in cells with depletion of endogenous Dis3. The Flag-tagged version of all these Dis3 variants could be expressed in comparable amount (Supplementary Figure S4), indicating that the catalytic site mutations did not significantly affect protein stability. In agreement with a suppressive effect of Dis3, the exogenous expression of Dis3-WT in the otherwise Dis3-depleted cells clearly retarded CG* degradation as compared to the empty vector control (Figure 2A and B [left]). Surprisingly, both Dis3-exo$^-$ and Dis3-endo$^-$ was as potent as Dis3-WT in slowing down the degradation kinetics of CG*, except for some slight differences observed for Dis3-exo$^-$ at the 3 h time point (Figure 2A and B [second-left and second-right]), suggesting that either its exo- or endo-ribonuclease activity was already sufficient. However, the completely catalytically-dead Dis3-exo$^-$endo$^-$ lost its ability to restrain CG* degradation, resulting in significantly accelerated CG* degradation as compared to cells expressing Dis3-WT (Figure 2A and B [right]). These results demonstrated that loss of both exo- and endo-ribonuclease activities of Dis3 was required to boost misfolded protein degradation and PQC activity.

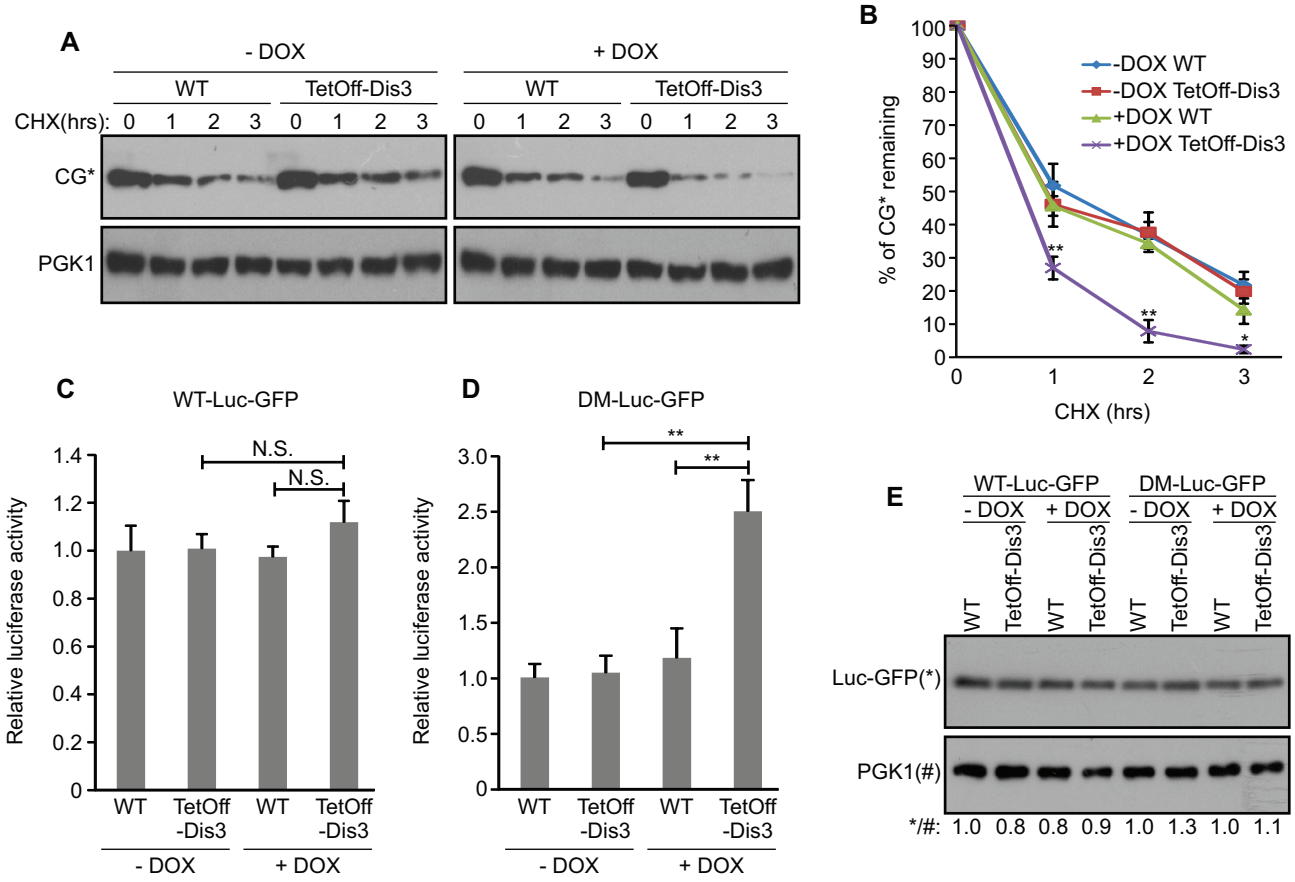

Figure 1. Dis3 is a negative regulator of PQC activity and protein folding capacity. (**A**) Immunoblotting analysis of CG* levels in WT and TetOff-Dis3 cells with or without DOX treatment at the indicated time points during CHX chase. PGK1 was detected as a loading control. (**B**) Degradation kinetics of CG* in cells with or without Dis3 depletion. CG* levels at different time points after CHX addition were quantified by ImageJ and then used to calculate the percentage of CG* remaining. Data are means ± SEM. $n = 4$ independent biological replicates. (**C**) Relative luciferase activity normalized to cell density in cells with or without Dis3 depletion expressing WT-Luc-GFP. Data are means ± SD. $n = 3$ independent biological replicates. (**D**) As in (**C**), but in cells expressing DM-Luc-GFP. (**E**) Western blot analysis of the relative levels of WT-Luc-GFP or DM-Luc-GFP in the indicated cells. The numbers below the blot represent the relative WT/DM-Luc-GFP levels normalized to PGK1 as measured by ImageJ. In all panels, N.S.: non-significant; $*P < 0.05$; $**P < 0.01$.

We then proceeded to test the effect of these Dis3 catalytic site mutations on DM-Luc-GFP folding. As a control, mutating its exoribonuclease site, endoribonuclease site, or both did not alter WT-Luc-GFP activity (Figure 2C). In accordance with Figure 1D, Dis3-depleted cells being transformed with empty vector showed around 2-fold higher DM-Luc-GFP activity as compared to cells with exogenous complementation of wild-type Dis3 (Figure 2D). Consistent with the analyses of CG* degradation, removal of neither the exo- nor the endo-ribonuclease activities of Dis3 enhanced DM-Luc-GFP signal, which could only be accomplished by the elimination of both activities (Figure 2D). Considering that these changes in Dis3 catalytic activities did not detectably affect WT/DM-Luc-GFP protein expression (Figure 2E), we inferred that the observed increase in DM-Luc-GFP activity was due to its improved folding efficiency, and that the ability of Dis3 to suppress protein folding capacity could only be abolished by mutating both its exo- and endo-ribonuclease sites.

Dis3 represses the expression of a subset of chaperones by rapid mRNA degradation

Since the loss of both exo- and endo-ribonuclease activities of Dis3 was sufficient to enhance PQC (Figure 2), we hypothesized that the underlying mechanism might involve the Dis3-mediated degradation of some mRNAs that encode important PQC factors. Accordingly, we selected a panel of 15 mRNAs encoding molecular chaperones and their cofactors, protein aggregases and disaggregases, E3 ligases, and ubiquitin binding receptor for the proteasome, which were all engaged in some steps of PQC, and then used qPCR to examine whether their steady-state levels were up-regulated in Dis3-depleted cells. Among these mRNAs, 6 of them exhibited <2-fold increase upon Dis3 depletion, including those encoding the cytosolic Hsp70s Ssa1, Ssb1 and Sse1, the Hsp90 chaperone Hsp82, the disaggregase Hsp104, as well as the E3 ligase Rsp5 (Figure 3A). The other mRNAs all showed more than 2-fold increment, with that encoding the Hsp40 Sis1, a cofactor of Hsp70,

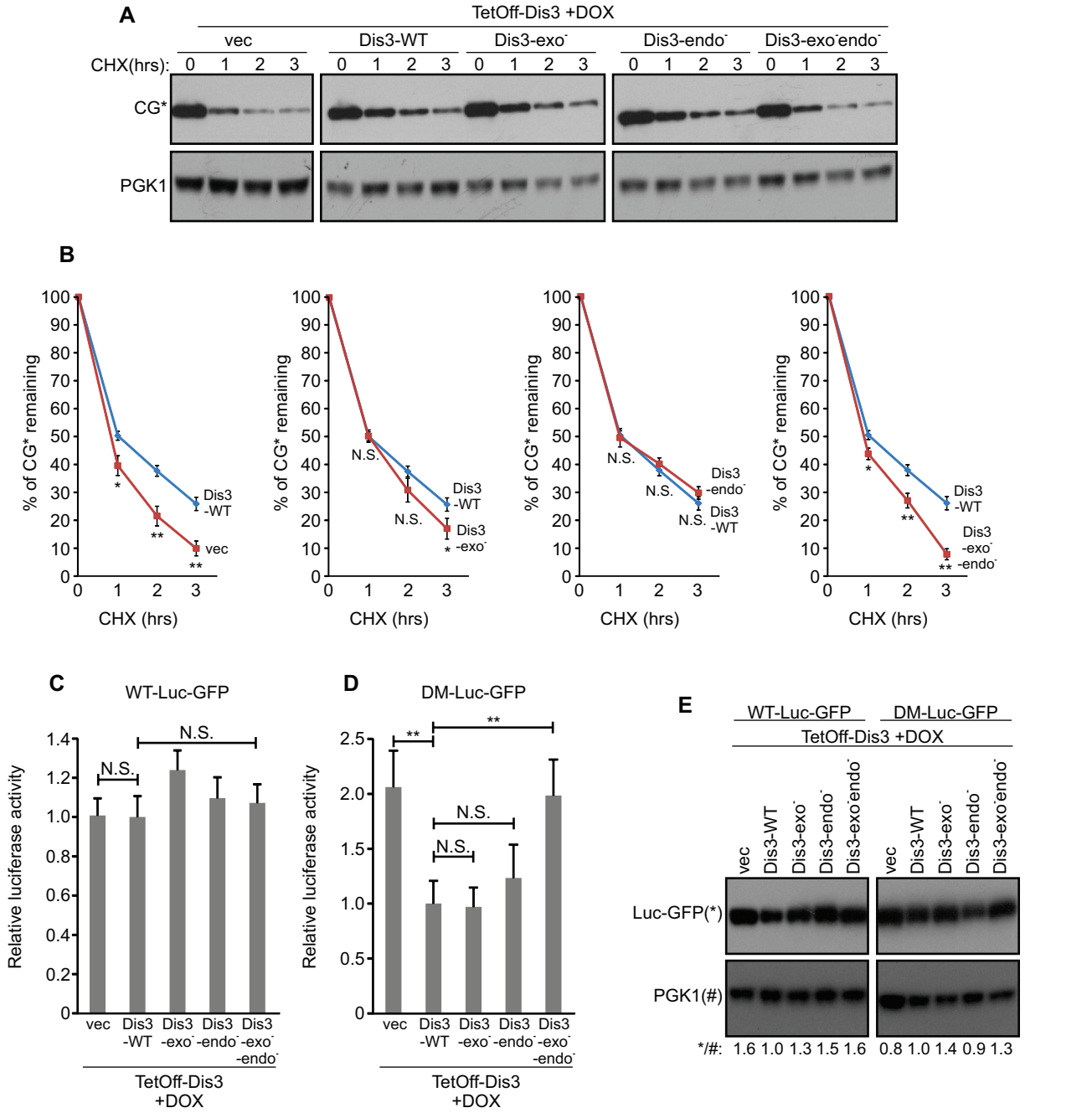

Figure 2. Loss of both 3′-5′ exoribonuclease and endoribonuclease activities of Dis3 is required to boost PQC activity and protein folding capacity. (**A**) CHX chase assay of CG* degradation in DOX-treated TetOff-Dis3 cells transformed with the indicated plasmids capable of expressing WT or catalytic site mutants of Dis3. (**B**) Comparison of CG* degradation rate between cells transformed with the indicated plasmids. Data are means ± SEM. $n = 6$ (for vec) or 7 (for others) independent biological replicates. (**C**) Relative luciferase activity in cells expressing WT-Luc-GFP and the indicated WT or mutated versions of Dis3. Data are means ± SD. n = 4 independent biological replicates. (**D**) As in (C), but in cells expressing DM-Luc-GFP. (**E**) Relative levels of WT-Luc-GFP or DM-Luc-GFP in the indicated cells as revealed by immunoblotting. The numbers below the blot show their relative WT/DM-Luc-GFP levels. In all panels, N.S.: non-significant; $*P < 0.05$; $**P < 0.01$.

having the greatest effect (10.4-fold), followed by those encoding two other Hsp70 cofactors Ydj1 (6.1-fold) and Fes1 (6.3-fold) (Figure 3A). The mRNAs of the protein aggregases Btn2 and Hsp42, the E3 ligases Ltn1, San1, and Ubr1, and the proteasome-associated ubiquitin binding receptor Dsk2 were also significantly up-regulated (Figure 3A). In contrast, deletion of *XRN1* had less than 2-fold effect on all these mRNAs with the exception of that encoding Ssb1 (Supplementary Figure S5), which was consistent with the observation that Xrn1 did not detectably regulate misfolded protein degradation and protein folding capacity (Supplementary Figure S3). Therefore, Dis3, but not Xrn1, was a potent suppressor of the mRNA expression of multiple PQC factors, including mostly molecular

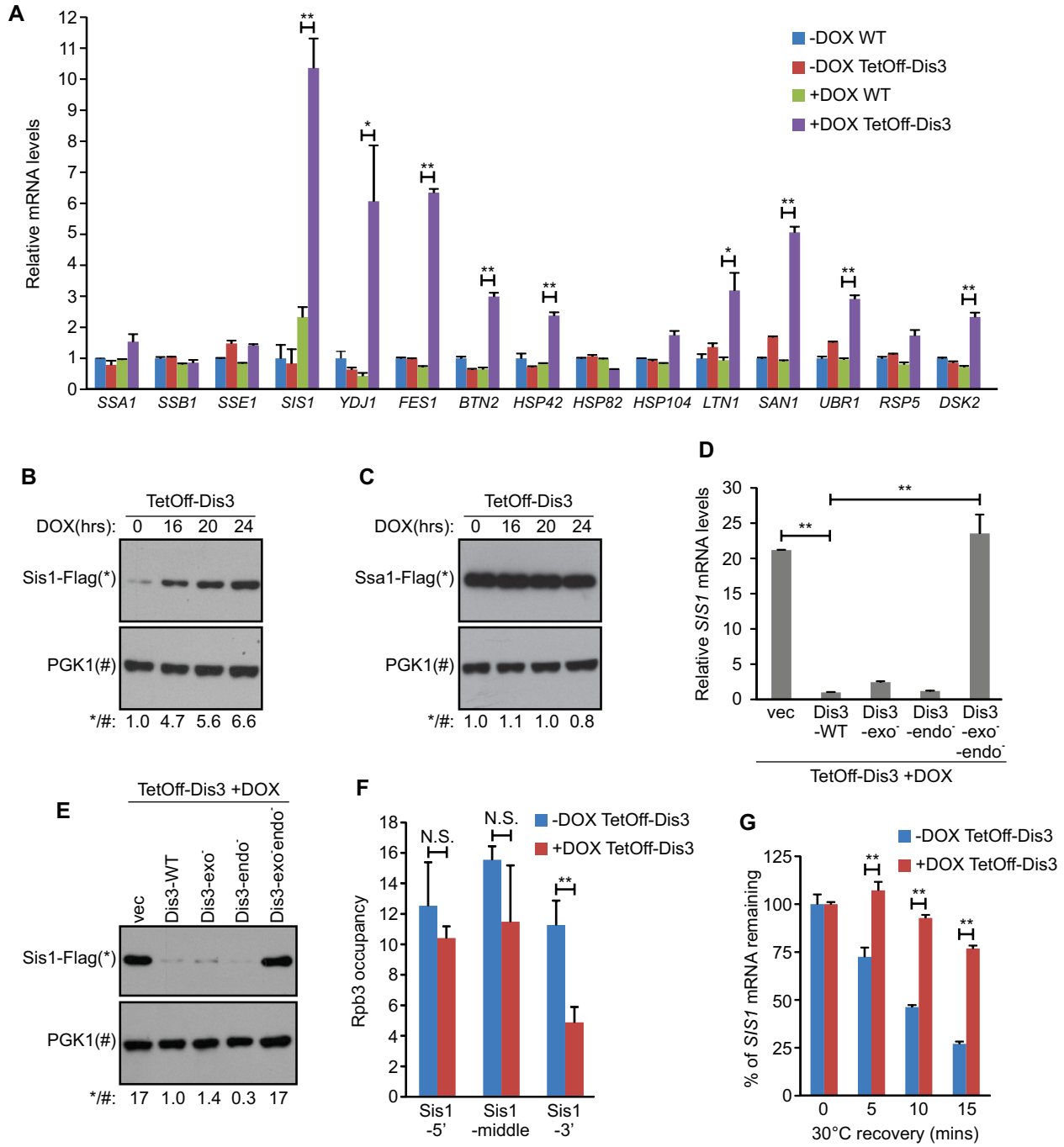

Figure 3. Dis3 represses the expression of a subset of chaperones such as Sis1 by rapid mRNA degradation. (**A**) Quantitative PCR (qPCR) measurement of the relative levels of the indicated mRNAs in cells with or without Dis3 depletion. Statistical analyses were done between the DOX-treated WT and TetOff-Dis3 cells if their difference for a particular mRNA was more than 2-fold. Data are means ± SD. n = 3 independent biological replicates. (**B**) Western blot analysis of relative Sis1-Flag expression in TetOff-Dis3 cells being treated with DOX for increasing amount of time. The numbers represent its relative levels as determined by ImageJ. (**C**) As in (B), but relative Ssa1-Flag expression was examined. (**D**) Relative *SIS1* mRNA abundance in DOX-treated TetOff-Dis3 cells transformed with plasmids expressing Dis3 with different catalytic activity profiles. Data are means ± SD. $n = 3$ independent biological replicates. (**E**) Relative Sis1-Flag levels in the indicated cells as depicted visually by the blot and quantitatively by the below numbers. (**F**) ChIP analysis of Rpb3 recruitment levels to the 5′, middle, and 3′ regions of the *SIS1* gene in TetOff-Dis3 cells with or without DOX treatment. Data are means ± SD. $n = 3$ independent biological replicates. (**G**) Degradation rate of excess *SIS1* mRNA when the indicated cells pre-treated with a 39°C heat shock for 20 min were returned to 30°C for recovery. The amount of *SIS1* mRNA at each time point was determined by qPCR, and then used to calculate the percentage of *SIS1* mRNA remaining as shown in the graph. Data are means ± SD. $n = 3$ independent biological replicates. In all panels, N.S.: non-significant; $*P < 0.05$; $**P < 0.01$.

chaperones that function as Hsp70 cofactors or protein aggregases, and also some E3 ligases involved in the ubiquitination of misfolded proteins (13–15,36). To identify additional mRNA substrates of Dis3, we performed a RNA sequencing experiment to compare the transcriptome of cells with or without Dis3 depletion. Among the 165 mRNAs with gene ontology terms 'protein folding' or 'ubiquitin-dependent protein catabolic process' in the *Saccharomyces* Genome Database (SGD), 126 mRNAs showed >2-fold accumulation in Dis3-depleted cells (Supplementary Table S4). These included not only most of the qPCR-verified Dis3 substrates (Figure 3A) like those encoding Sis1, Ydj1, and Fes1, but also mRNAs of the Hsp40 Xdj1, the E3 ligases Cul3, Dma1 and Psh1, the cytosolic Hsp70 Ssa3, the inner nuclear membrane PQC factor Asi3, the endoplasmic reticulum-associated degradation (ERAD) factor Ufd1, and the protein aggregase Cur1, suggesting a broad role of Dis3 in suppressing the expression of mRNAs encoding proteins involved in diverse PQC pathways.

Since the *SIS1* mRNA showed the strongest up-regulation among all qPCR-tested mRNAs (Figure 3A), we performed some further analyses on Sis1 expression. Upon Dis3 depletion, the amount of Sis1 protein, which was C-terminally tagged by Flag without changing the 3′-UTR sequence of its mRNA, markedly increased in a time-dependent manner to >6-fold when Dis3 had been depleted for 24 h (Figure 3B). As a control, the expression level of Flag-tagged Ssa1, of which the corresponding mRNA only showed limited increase in Dis3-depleted cells (Figure 3A), did not detectably change over the course of this experiment (Figure 3C). These results demonstrated that Dis3 robustly inhibited the protein expression of Sis1 by down-regulating its mRNA. Similar effect was expected for other chaperones and PQC factors of which the abundance of their corresponding mRNAs were also responsive to Dis3 depletion.

We then investigated the importance of the 3′-5′ exoribonuclease and endoribonuclease activities of Dis3 in repressing Sis1 expression. Complementation by exogenous Dis3-WT greatly diminished the expression levels of both *SIS1* mRNA (Figure 3D) and its protein (Figure 3E) in the otherwise Dis3-depleted cells, confirming their negative regulation by Dis3. Although both Dis3-exo$^-$ and Dis3-endo$^-$ could restore *SIS1* mRNA (Figure 3D) and its protein (Figure 3E) expression almost as efficiently as Dis3-WT, the Dis3-exo$^-$endo$^-$ mutant completely failed to lessen their expression levels (Figure 3D and E), indicating that either its exo- or endo-ribonuclease activity was required and sufficient to subdue the expression of Sis1. Therefore, the requirement of Dis3 ribonuclease activities was alike in both its regulation of PQC activity and Sis1 abundance.

The steady-state level of a mRNA depends on the balance between its rate of synthesis by RNA polymerase II-mediated transcription and rate of degradation by the action of various ribonucleases. To elucidate whether the increased *SIS1* mRNA expression in Dis3-depleted cells (Figure 3A and D) was due to enhanced transcription and/or reduced degradation, we measured the occupancy of the RNA polymerase II subunit Rpb3 along the *SIS1* gene, as well as monitored the decay of excess *SIS1* mRNA during heat stress recovery. Chromatin immunoprecipitation (ChIP) analysis revealed that Rpb3 occupancy, which represented transcriptional activity (37,38), was similar in cells with and without Dis3 depletion at the 5′-end and middle region of the *SIS1* gene, and that at the 3′-end was even decreased upon Dis3 depletion (Figure 3F), implying that the down-regulation of *SIS1* mRNA by Dis3 was not mediated by changes in transcription rate. On the other hand, the degradation of excess *SIS1* mRNA during recovery from an acute heat stress was substantially impeded in Dis3-depleted cells (Figure 3G). This indicated that the increased *SIS1* mRNA abundance in response to Dis3 depletion was mainly due to its retarded degradation, which was consistent with the above findings that the suppression of *SIS1* mRNA expression by Dis3 was dependent on its capability to function as a ribonuclease (Figure 3D).

Sis1 has recently been shown to facilitate the degradation of misfolded proteins including CG* by promoting their nuclear transport (12,39,40). To verify whether the increased Sis1 abundance in Dis3-depleted cells (Figure 3B and E) contributed to accelerated CG* degradation (Figure 1A), its degradation kinetics in cells with or without overexpression of HA-tagged Sis1 were compared. As expected, Sis1-HA overexpression stimulated CG* degradation remarkably (Supplementary Figure S6), suggesting that the functionality of Sis1 in facilitating CG* degradation could be recapitulated in our experimental system, and that the elevated amount of Sis1 in Dis3-depleted cells was at least partially responsible for the enhanced degradation of CG*. In addition to the *SIS1* mRNA, Dis3 depletion also resulted in the up-regulation of mRNAs encoding some other chaperones and PQC factors (Figure 3A), such as the Hsp70 cofactors Ydj1 and Fes1 as well as the E3 ligases San1 and Ubr1, which were all involved in misfolded protein degradation (13–17). Therefore, it was reasonable to assume that the gain of these chaperones and PQC factors upon Dis3 depletion might also contribute to accelerated CG* degradation. Collectively, our findings demonstrated that Dis3 repressed the expression of a number of chaperones and PQC factors such as Sis1 by rapidly degrading their corresponding mRNAs, and consequently suppressed misfolded protein degradation and PQC activity.

An AU-rich element (ARE) found in the 3′-UTR of *SIS1* mRNA couples it to Dis3-mediated regulation

Given that only a subset of the tested mRNAs was down-regulated by Dis3 (Figure 3A and Supplementary Table S4), we inferred that Dis3 did not non-selectively target all mRNAs for degradation but instead showed some substrate specificity. The metabolism of many eukaryotic mRNAs is controlled by different *cis*-regulatory elements, such as the AU-rich elements (AREs) commonly located within the 3′-UTR. The AREs are short sequence elements rich in adenosine and uridine bases with most of them containing the 'AUUUA' motif (41), and can specifically direct the mRNAs to subsequent degradation by the RNA exosome (9). Interestingly, when we searched for the existence of AREs within the first 100bp of the 3′-UTR belonging to those tested mRNAs, we found that the presence of 'AUUUA' motif was enriched in mRNAs that showed >2-fold increase in response to Dis3 depletion in qPCR analysis (Figure 4A). Moreover, 57.1% of mRNAs (16 out of 28) that showed >3.5-fold in-

A

	Number of AREs	Starting position	Sequences
mRNAs that show less than 2-fold increase upon Dis3 depletion			
SSA1	0	N/A	N/A
SSB1	0	N/A	N/A
SSE1	0	N/A	N/A
HSP82	0	N/A	N/A
HSP104	0	N/A	N/A
RSP5	1	24	UUAUUUAUG
mRNAs that show more than 2-fold increase upon Dis3 depletion			
SIS1	1	38	AAAUUUAUC
YDJ1	1	38	UCAUUUAUU
FES1	1	68	ACAUUUAUU
BTN2	0	N/A	N/A
HSP42	2	31	ACAUUUAUA
		37	AUAUUUAUA
LTN1	0	N/A	N/A
SAN1	0	N/A	N/A
UBR1	1	88	UUAUUUAUU
DSK2	1	54	AUAUUUAAU

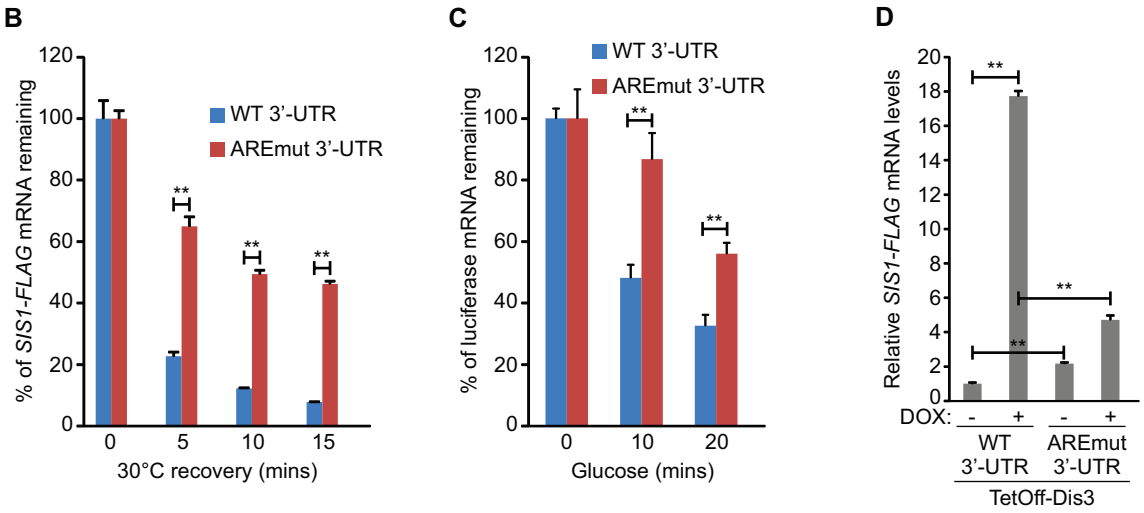

Figure 4. An AU-rich element (ARE) found in the 3′-UTR of *SIS1* mRNA couples it to Dis3-mediated regulation. (**A**) A table showing the number of ARE-representing 'AUUUA' motifs within the first 100 bp of 3′-UTR sequences of the indicated mRNAs. Their starting position and surrounding sequences are also shown. (**B**) Degradation kinetics of excess *SIS1-FLAG* mRNA containing the WT or ARE-mutated 3′-UTR during the 30°C recovery after an acute heat shock at 39°C for 20 min. Data are means ± SD. $n = 3$ independent biological replicates. (**C**) Decay of luciferase mRNA with the indicated 3′-UTR after rapid transcriptional shut off by 4% glucose. Data are means ± SD. $n = 3$ independent biological replicates. (**D**) Relative levels of *SIS1-FLAG* mRNA containing the indicated 3′-UTR in cells with or without depletion of Dis3. Data are means ± SD. $n = 3$ independent biological replicates. In all panels, N.S.: non-significant; $*P < 0.05$; $**P < 0.01$.

crease in RNA sequencing contained the 'AUUUA' motif, as compared to only 26.2% (36 out of 137) for those less up-regulated mRNAs (Supplementary Table S4), with this difference in ARE distribution proved to be statistically significant by Pearson's chi-squared test ($P = 0.001358$). Therefore, we hypothesized that the specificity of Dis3-mediated degradation towards most of its substrates might be conferred by their AREs.

The *SIS1* mRNA contained one ARE in its 3′-UTR (Figure 4A). During recovery from an acute heat stress, the excess *SIS1-FLAG* mRNA with WT 3′-UTR was swiftly degraded, with a half-life of much less than 5 min (Figure 4B). Mutation of its ARE from 'AUUUA' to 'AGGGA' (AREmut) significantly delayed *SIS1-FLAG* mRNA degradation (Figure 4B), demonstrating its ability to reduce *SIS1-FLAG* mRNA stability. We also attached the WT or AREmut *SIS1* 3′-UTR downstream of a luciferase mRNA with its expression driven by a galactose-inducible promoter. Upon rapid transcriptional shut off by the addition of glucose, the luciferase mRNA was degraded in an ARE-dependent manner (Figure 4C), providing further evidence to support the destabilization effect of the *SIS1* ARE.

To understand whether the ARE-enhanced *SIS1-FLAG* mRNA degradation (Figure 4B) was mediated by Dis3, we investigated how Dis3 depletion modified the effect of ARE mutation on *SIS1-FLAG* mRNA expression. In control cells without Dis3 depletion, mutating the ARE led to around 2-fold increase in *SIS1-FLAG* mRNA level (Figure 4D), which agreed with the destabilization effect of the ARE (Figure 4B). Surprisingly, although Dis3 depletion in cells with WT 3′-UTR resulted in the expected huge up-regulation of *SIS1-FLAG* mRNA (Figure 4D), its effect in cells with AREmut 3′-UTR was relatively much smaller (Figure 4D), suggesting that *SIS1-FLAG* mRNA without

the ARE was less dependent on Dis3 for degradation and likely be more preferentially degraded by other ribonucleases such as Xrn1 or Rrp6 which was still fully active in Dis3-depleted cells. These findings not only proved the importance of the ARE to couple *SIS1* mRNA to Dis3-mediated regulation, but also underlay an experimental system that would be used later in this study for testing whether *SIS1* mRNA expression might be controlled by physiological changes in Dis3 protein level.

Loss of Sis1 and Ssa1/2 availability during heat stress leads to the ubiquitination and proteasomal degradation of Dis3

We were very curious about whether the Dis3-mediated degradation of chaperone mRNAs might be suppressed during heat stress to achieve their stabilization. Indeed, GFP-tagged Dis3 was obviously down-regulated during heat stress at 39°C (Figure 5A) without any detectable differences in its solubility (Supplementary Figure S7A) and subcellular localization (Supplementary Figure S7B). Similar down-regulation could also be observed for Myc-tagged Dis3 (Supplementary Figure S8A), suggesting that the instability of Dis3-GFP was not caused by the GFP tag. The down-regulation of Dis3-GFP was solely due to its degradation by the proteasome, as treatment of the proteasomal inhibitor MG132 completely blocked the reduction in Dis3-GFP abundance (Figure 5B). Consistent with this, Dis3-GFP was ubiquitinated during heat stress (Figure 5C), thereby committing it to proteasomal degradation.

Bulk transcription is inhibited during heat stress (42). However, the possible transcriptional attenuation of the *DIS3* gene could only partially explain the heat stress-induced reduction in Dis3 protein level, as abundance of the Dis3-Myc protein expressed from a TetOff promoter showed much faster decline during heat stress as compared to that after complete transcriptional repression by DOX (Supplementary Figure S8B). To determine whether Dis3 degradation was also triggered by the decline in chaperone availability during heat stress, we asked if the restoration of chaperone availability by their overexpression could arrest Dis3 degradation. With this in mind, we overexpressed HA-tagged Sis1, which was subjected to Dis3-mediated regulation (Figure 3), and also Ssa1, which was shown to bind to Dis3 together with its nearly identical paralog Ssa2 in a high-throughput analysis (43), and found that their strong overexpression really retarded Dis3 degradation (Figure 5D). Moreover, the abundance of Dis3 was tremendously reduced to barely detectable level in cells with Sis1 depletion (Figure 5E) or *SSA1* and *SSA2* double deletion (Figure 5F), showing that Dis3 required the presence of available Sis1 and Ssa1/2 to maintain its stability. More importantly, co-immunoprecipitation analyses revealed the previously unreported binding between Dis3 and Sis1 (Figure 5G) and confirmed the already documented binding (43) between Dis3 and Ssa1/2 (Figure 5I), which were all obstructed during heat stress (Figure 5H and J). Therefore, the regulatory mechanism of Dis3 stability was highly similar to that of Hsf1 activity. Dis3 normally remained stable by binding to Sis1 and Ssa1/2, which was titrated away during heat stress, and thereby released Dis3 for subsequent ubiquitination and proteasomal degradation.

Dis3 degradation during heat stress results in the stabilization of chaperone mRNAs

To explore the functionality of Dis3 degradation, we first measured the changes in *SIS1*, *YDJ1* and *FES1* mRNA stability during heat stress by monitoring their degradation kinetics after addition of the transcriptional inhibitor thiolutin. As inferred from the rapid degradation of these mRNAs by Dis3 (Figure 3) and the heat shock-mediated reduction of Dis3 level (Figure 5A), their stability greatly increased after 30 min of heat stress, as compared to that in cells being heat shocked for just 5 min (Figure 6A–C). However, it is worthwhile to note that although the comparisons between their relative stabilities were valid in this experiment, their absolute stabilities were likely overestimated as thiolutin also had a secondary effect of inducing some degree of stress response before completely blocking transcription (44). We then aimed to verify the relationship between chaperone mRNA stabilization and Dis3 degradation. To this end, we delayed the reduction in overall Dis3 level by overexpressing HA-tagged Dis3, which was only swiftly degraded after 30 min of heat stress (Figure 7A). Therefore, we focused on examining the induction of *SIS1*, *YDJ1*, and *FES1* mRNAs at the 15 and 30 min time points, and found that these were all significantly diminished upon Dis3-HA overexpression (Figure 7B–D), suggesting the importance of rapid Dis3 removal to an optimal heat stress response. As a negative control, the *SSA1* and *HSP82* mRNAs, which were much less dependent on Dis3 for degradation (Figure 3A), showed only moderately reduced or even unchanged induction fold at the 15 and 30 min time points respectively upon overexpression of Dis3-HA (Supplementary Figure S9A and B).

Mutation of the ARE within the *SIS1-FLAG* 3′-UTR lessened the effect of Dis3 reduction on *SIS1-FLAG* mRNA level (Figure 4D). When the cells expressing *SIS1-FLAG* mRNA with WT 3′-UTR were subjected to heat stress, its expression was rapidly induced during the first 15 min and then slowly down-regulated (Figure 7E) with decreasing reduction rate over time (Figure 7F). Mutation of the ARE had no significant changes on *SIS1-FLAG* mRNA level at 15 and 30 min after heat stress (Figure 7E), but resulted in its moderately faster down-regulation thereafter (Figure 7E) as indicated by its relatively greater reduction rate at all time points after 30 min (Figure 7F), and consequently could not sustain the high expression level of Sis1-Flag protein at the 90 min time point (Figure 7G). No significant effects on the transcription activity pattern during heat stress were caused by the ARE mutation (Supplementary Figure S10A), suggesting that the differences in *SIS1-FLAG* mRNA reduction rate were most likely due to changes in mRNA stability rather than transcription. Since the removal of ARE from *SIS1-FLAG* mRNA lessened its sensitivity to Dis3 depletion (Figure 4D), and at the same time reduced its stability in the later stages of heat stress (Figure 7E and F), we concluded that *SIS1* mRNA stabilization re-

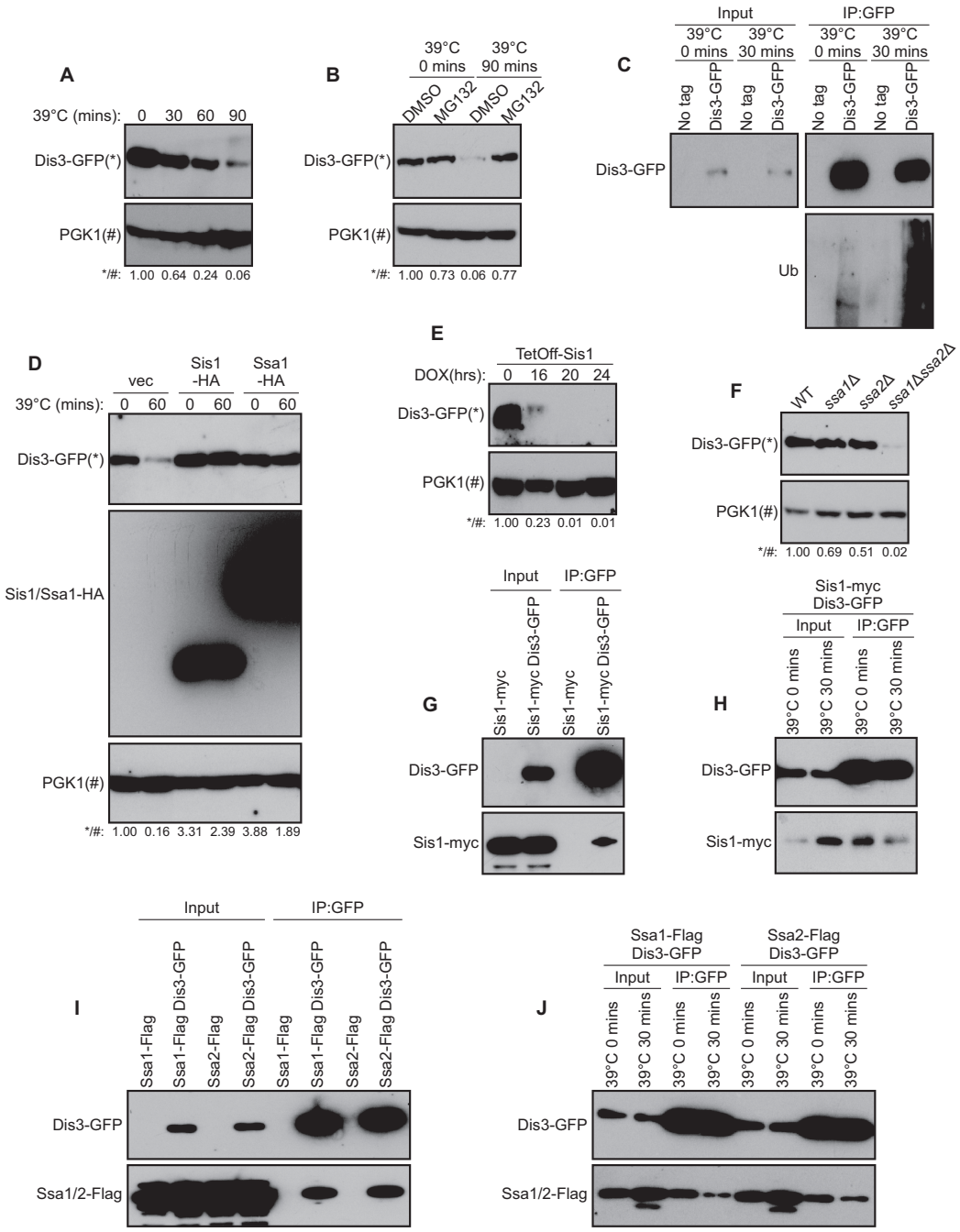

Figure 5. Loss of Sis1 and Ssa1/2 availability during heat stress leads to the ubiquitination and proteasomal degradation of Dis3. (**A**) Western blot detection of Dis3-GFP levels at different time points during 39°C heat shock. The numbers below the blot show their relative abundance. (**B**) Analysis of the effect of MG132 on Dis3-GFP down-regulation during heat shock. Either MG132 (80 μM) or its solvent control DMSO was added to *PDR5*-knockout cells expressing Dis3-GFP, followed by an immediate heat shock at 39°C with cell harvesting performed at 0 or 90 min thereafter. The relative Dis3-GFP levels in these cells are represented by the numbers at the bottom. (**C**) Detection of Dis3-GFP ubiquitination in cells with or without 39°C heat shock for 30 min. Dis3-GFP was immunoprecipitated by anti-GFP antibody, and then immunoblotting detection of Dis3-GFP and ubiquitin chain in the input (5%) and immunoprecipitated (IP) samples was performed. Note that we cannot exclude the possibility that the ubiquitination signal comes from some ubiquitinated proteins associated with Dis3-GFP, although it is unlikely since Dis3 is in general not involved in the protein ubiquitination and degradation pathways, and not many proteins have a size greater than that of Dis3-GFP (∼140 kDa). (**D**) Dis3-GFP-expressing cells with or without overexpression of Sis1-HA or Ssa1-HA, as indicated, were subjected to immunoblotting analysis of Dis3-GFP levels after they had been heat shocked for 0 or 60 min. The numbers below represent its quantified relative levels. (**E**) Dis3-GFP expression in cells subjected to Sis1 depletion for an increasing amount of time. The numbers below the blot show Dis3-GFP abundance relative to control cells without Sis1 depletion. (**F**) Dis3-GFP expression in cells with the indicated deletion of the *SSA1* and/or *SSA2* genes. The numbers below the blot show Dis3-GFP abundance relative to control cells without gene deletions. (**G**) Co-immunoprecipitation analysis of the binding between Dis3-GFP and Sis1-myc. Dis3-GFP was first immunoprecipitated by anti-GFP antibody, followed by immunoblotting detection of Dis3-GFP and Sis1-myc in the input (5%) and immunoprecipitated (IP) samples. (**H**) Similar to (**G**), but was performed in cells with further deletion of *PDR5* and addition of MG132 just prior to heat shock. Only 0.5% of input was loaded. (**I** and **J**) Similar to (**G** and **H**) respectively, but the interaction between Dis3-GFP and Ssa1/2-Flag was analyzed.

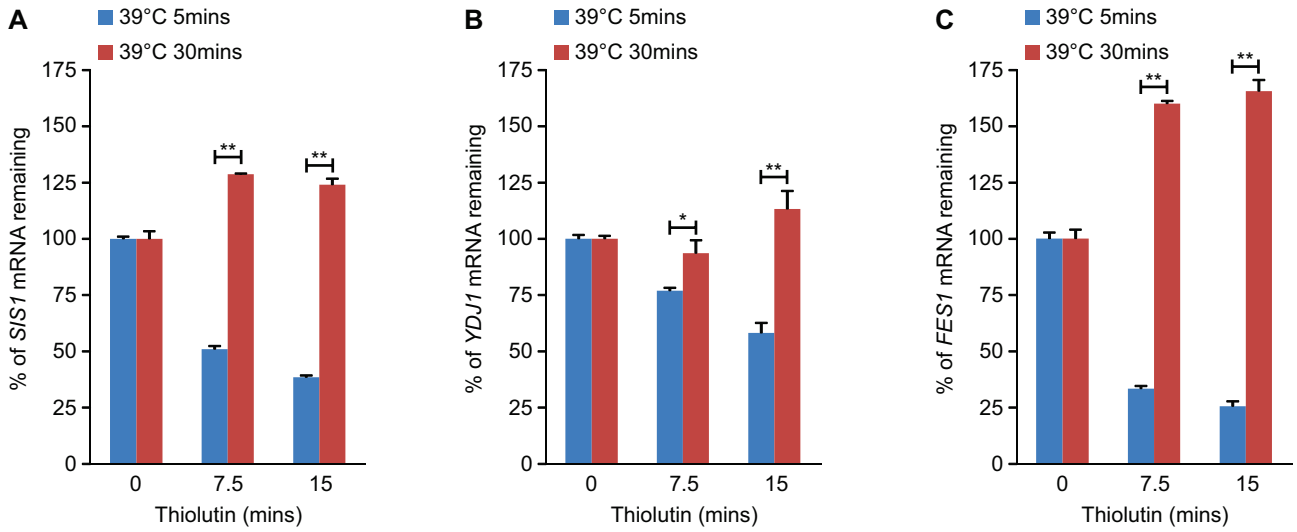

Figure 6. Some chaperone mRNAs are stabilized during heat stress. (A–C) Degradation kinetics of *SIS1* (**A**), *YDJ1* (**B**) and *FES1* (**C**) mRNAs when their transcription was stopped by thiolutin after being heat shocked at 39°C for the indicated amount of time. Data are means ± SD. $n = 3$ independent biological replicates. In all panels, N.S.: non-significant; $*P < 0.05$; $**P < 0.01$.

quired its responsiveness to Dis3 degradation (Figure 5A), or in other words, the proteasomal degradation of Dis3 during heat stress triggered the stabilization of *SIS1* mRNA.

PolyQ-expanded huntingtin diminishes the stabilization of chaperone mRNAs during heat stress by retarding Dis3 degradation

It had been reported that polyQ-expanded huntingtin could suppress the induction of chaperone expression during heat stress (27), which might lead to the gradual decline of proteostasis capacity in Huntington's disease. We generated a yeast model of Huntington's disease by expressing the N-terminally Myc-mCherry-tagged pathogenic huntingtin exon 1 fragment with 96 glutamines (Myc-mCherry-Htt96Q) or the control with 25 glutamines (Myc-mCherry-Htt25Q), and investigated whether polyQ-expanded huntingtin might modify the Dis3 degradation-mediated chaperone mRNA stabilization and thereby contribute to the impaired heat stress response. Interestingly, the degradation of Dis3-GFP (Figure 8A) and Dis3-Flag (Supplementary Figure S8C) upon heat stress was clearly blocked in cells expressing Myc-mCherry-Htt96Q, suggesting that chaperone mRNA stabilization might be consequently affected, which was soon validated by the observation that the decay of *SIS1*, *YDJ1* and *FES1* mRNAs starting from 30 min after heat stress were all significantly faster in these cells (Figure 8B–D). Their faster decay was probably due to reduced mRNA stability but not lower transcription activity, as Myc-mCherry-Htt96Q expression did not significantly alter the changes in their transcription rate during heat stress (Supplementary Figure S10B–D). Taken together, these findings demonstrated that polyQ-expanded huntingtin disrupted the stabilization of these chaperone mRNAs during heat stress by impeding the timely degradation of Dis3, which might represent one of the mechanisms that were responsible for the impaired heat stress response in Huntington's disease.

DISCUSSION

In this study, we identified a post-transcriptional negative feedback loop that regulates proteostasis through the Dis3 ribonuclease, and characterized how polyQ-expanded huntingtin disrupts this pathway and thereby contributes to its suppression of the heat stress response. In this feedback loop (Figure 9), the PQC activity and protein folding capacity in unstressed cells are restrained by Dis3 through its rapid degradation of the mRNAs encoding a subset of important molecular chaperones and PQC factors, such as the Hsp70 cofactors Sis1, Ydj1 and Fes1 that are known to be involved in misfolded protein degradation. This efficient degradation of *SIS1* mRNA is at least partially conferred by an ARE in its 3′-UTR, and requires only the 3′-5′ exoribonuclease or endoribonuclease activity of Dis3. The stable expression of Dis3 in this proteostatically healthy condition is maintained by its binding to available Sis1 and Ssa1/2, which are titrated away by the huge amount of misfolded proteins during proteostatically imbalanced condition such as heat stress, resulting in the release of Dis3 for subsequent ubiquitination and proteasomal degradation. Consequently, the mRNAs encoding many chaperones or PQC factors such as Sis1, Ydj1, and Fes1 are stabilized and may then be translated into their corresponding proteins which can handle the misfolded polypeptides and restore proteostasis. In addition, the possible stabilization of several E3 ligase mRNAs that are suggested to be Dis3 targets by RNA sequencing (Supplementary Table S4), such as that of San1, Ubr1, Cul3, Dma1 and Psh1, may in turn enhance Dis3 degradation by increasing its ubiquitination. However, the timely removal of Dis3 is impeded by polyQ-expanded huntingtin, which allows the continuation of chaperone mRNA degradation and therefore leads to an impaired heat stress response.

The stabilization of chaperone mRNAs during heat stress may enhance cell survival by conserving those chaperone mRNAs that have already been synthesized and thereby

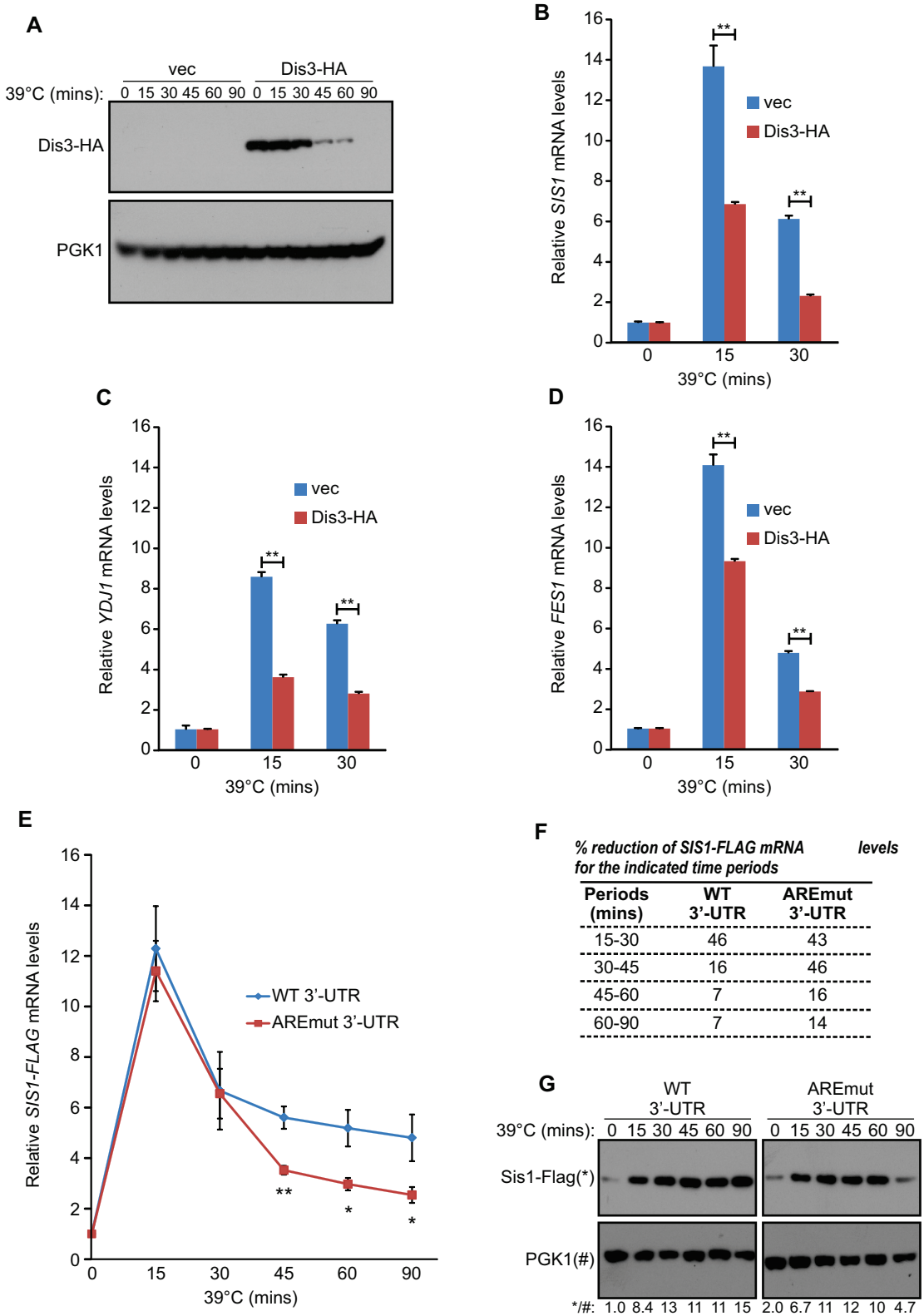

Figure 7. Dis3 degradation during heat stress is required for the optimal induction and stabilization of some chaperone mRNAs. (**A**) Western blot analysis of Dis3-HA levels during 39°C heat shock. (B–D) Fold of induction of *SIS1* (**B**), *YDJ1* (**C**) and *FES1* (**D**) mRNAs in cells with or without Dis3-HA overexpression after 39°C heat shock for 15 or 30 min. Data are means ± SD. $n = 3$ independent biological replicates. (**E**) Heat stress response in the levels of *SIS1-FLAG* mRNAs containing the indicated 3′-UTRs. Data are means ± SEM. $n = 4$ independent biological replicates. (**F**) Percentage reduction of the level of *SIS1-FLAG* mRNA with or without ARE mutation during the indicated time periods as calculated from the data shown in (E). (**G**) Immunoblotting analysis of the heat stress response of Sis1-Flag proteins encoded by *SIS1* mRNAs with or without ARE mutation. The numbers below the blot show their relative levels. In all panels, N.S.: non-significant; $*P < 0.05$; $**P < 0.01$.

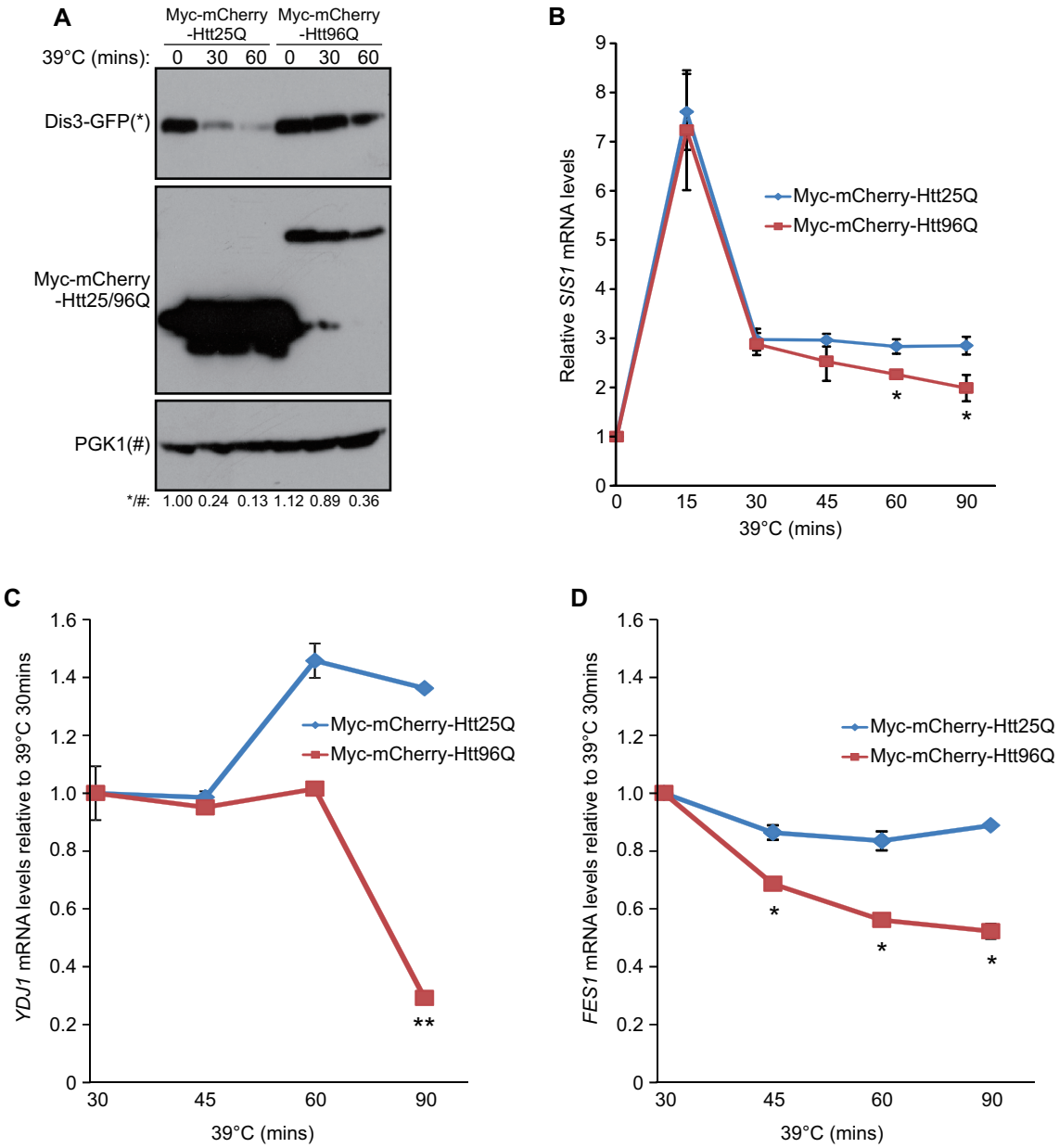

Figure 8. PolyQ-expanded huntingtin diminishes the stabilization of chaperone mRNAs during heat stress by retarding Dis3 degradation. (**A**) Degradation of Dis3-GFP during 39°C heat shock in cells expressing Myc-mCherry-Htt25Q or Myc-mCherry-Htt96Q. The numbers at the bottom represent their relative abundance. (**B**) Relative levels of *SIS1* mRNA at different time points during 39°C heat shock in Myc-mCherry-Htt25Q- or Myc-mCherry-Htt96Q-expressing cells were determined by qPCR. Data are means ± SEM. $n = 3$ independent biological replicates. (C and D) The levels of *YDJ1* (**C**) and *FES1* (**D**) mRNAs relative to that at the 39°C 30 min time point in cells expressing Myc-mCherry-Htt25Q or Myc-mCherry-Htt96Q. Data are means ± SEM. $n = 3$ independent biological replicates. In all panels, N.S.: non-significant; $^*P < 0.05$; $^{**}P < 0.01$.

allowing allocation of the limited amount of cellular resources and energy to combating the deleterious misfolded proteins. Also, the mRNA stabilization pathway may partially complement the canonical Hsf1-mediated transcriptional activation pathway when Hsf1 expression, trimerization, nuclear translocation, phosphorylation, or other steps leading to the stimulation of its activity are blocked, for example during aging (45,46). Another advantage of this pathway is that it enables the cells to respond to the decline of RNA degradation activity, or the accumulation of aberrant RNAs that may compete for Dis3-mediated degradation, by the concomitant stabilization of chaperone mRNAs. This can never be achieved by the Hsf1 pathway before these aberrant RNAs are translated into potentially toxic misfolded proteins.

It is very curious that either the exo- or endo-ribonuclease activities of Dis3 is already sufficient to restrain *SIS1* mRNA at its basal level (Figure 3D). While its exoribonuclease activity should enable the complete degradation of *SIS1* mRNA starting from the 3′-end, how its endoribonuclease activity can equally suppress *SIS1* mRNA expression is more difficult to understand. The most likely mecha-

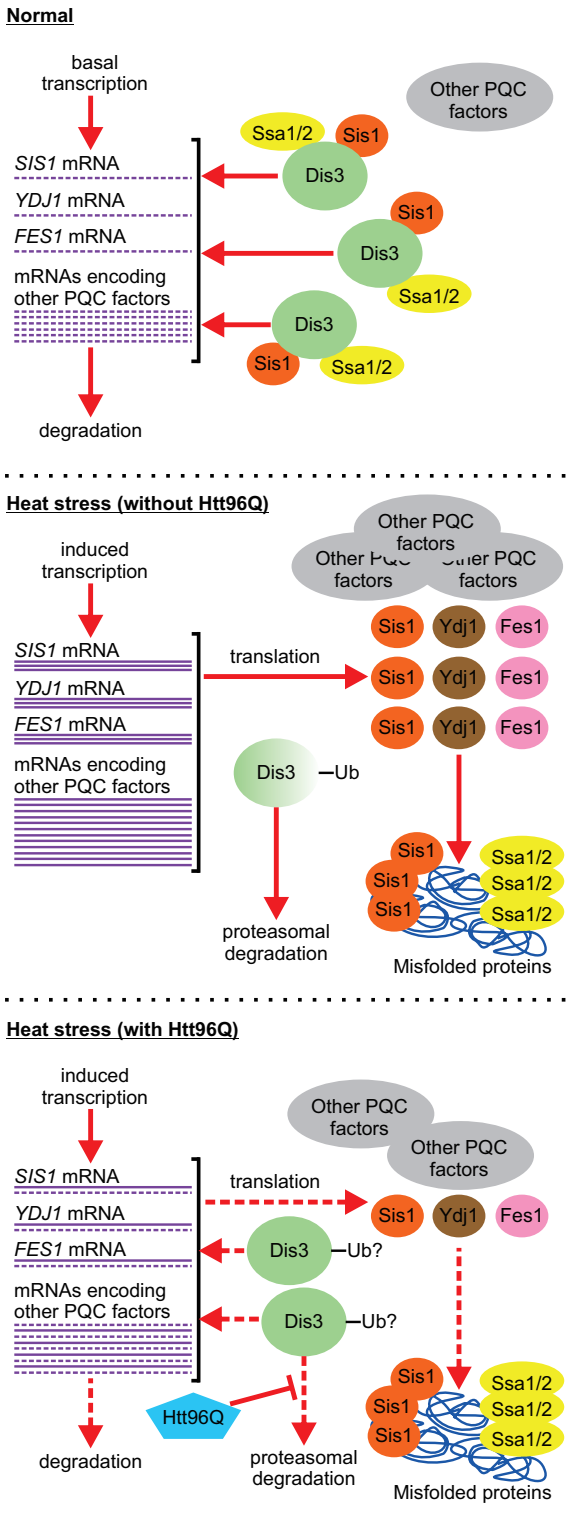

Figure 9. A schematic diagram of our proposed model illustrating how the identified post-transcriptional negative feedback loop responds to heat stress and how it is disrupted by polyQ-expanded huntingtin.

nism is that its endoribonuclease activity may cut the *SIS1* mRNA internally and thereby generate entry point(s) for the subsequent action of other ribonucleases such as Xrn1. Further experiments are required to verify this hypothesis and to pinpoint the exact cutting site(s) within *SIS1* mRNA.

It is certainly of great interest to understand the mechanism of Dis3 ubiquitination upon heat stress. To this end, it will be necessary to define the ubiquitination site(s) on Dis3, and to specify the responsible E3 ligase(s). One probable candidate E3 ligase is Rsp5, which targets cytosolic misfolded proteins for ubiquitination during heat stress (47), and has been shown to ubiquitinate Dis3 in an *in vitro* ubiquitination screening of Rsp5 substrates (48). Extending from this, it may also be worthwhile to determine whether polyQ-expanded huntingtin retards Dis3 degradation by sequestrating or inhibiting the responsible E3 ligase(s). Interestingly, it has been reported that Rsp5 colocalizes with polyQ-expanded huntingtin aggregates (49), suggesting that some functional interplay or physical interaction between them may exist.

A key question to our findings and proposed model is of course whether these may also be conserved in human cells. There are three human homologs of yeast Dis3, namely Dis3, Dis3L, and Dis3L2, which have different subcellular localization and ribonuclease activities (8). While yeast Dis3 can be found in both the nucleus and cytoplasm, human Dis3 has a predominantly nuclear localization while Dis3L and Dis3L2 are exclusively cytoplasmic (50,51). Both Dis3 and Dis3L have been shown to associate with the nuclear and cytoplasmic exosome respectively, while Dis3L2 functions independently from the core exosome (52). All of these three human Dis3 homologs possess 3′-5′ exoribonuclease activity, with only Dis3 also has the ability to function as an endoribonuclease. Given this heterogeneity among their biological properties, it is highly tempting to investigate which human Dis3 homologs are required for and how they cooperate with each other in the regulation of PQC activity, as well as to determine which Dis3 homologs are actively degraded during heat stress or other proteotoxic conditions. Our work using the budding yeast model has suggested the probable existence of a similar post-transcriptional pathway for regulating proteostasis in human cells, and has certainly provided a general view of its molecular mechanisms and functionality.

While polyQ-expanded huntingtin suppresses the heat stress response at least partially by reducing Hsf1 expression (27) and impeding Dis3 degradation (this work), several studies have suggested that pharmacological activation of the heat stress response by different Hsp90 inhibitors may mitigate its cellular toxicity by altering its aggregation through the action of the increased amount of chaperones (28–30). Based on our findings, we propose that the chemical inhibition of Dis3 should in principle also be able to boost the expression of some chaperones, and may therefore represent an alternative strategy to treat Huntington's or other neurodegenerative diseases. Unfortunately, there are still no reported Dis3 inhibitors at present. Therefore, chemical inhibitors against human Dis3, Dis3L and Dis3L2 may be developed and then tested for their ability to augment chaperones expression and restore proteostasis in cel-

lular and mouse models of neurodegenerative diseases, an extremely fascinating possibility that awaits further investigation.

SUPPLEMENTARY DATA

Supplementary Data are available at NAR Online.

ACKNOWLEDGEMENTS

We thank all members of the Jin's laboratory for discussions and technical support. We also thank Prof. F. Ulrich Hartl for his helpful comments on this study. In addition, we acknowledge Prof. J. Scott Butler for providing the TetOff-Dis3 as well as its corresponding control yeast strains. Finally, we appreciate Dr Hin Kwok and other staff of the Centre for Genomic Sciences, The University of Hong Kong, for their help in RNA sequencing.

FUNDING

Hong Kong Health and Medical Research Fund [16150342 to K.-Y.E.K.]. Funding for open access charge: Hong Kong Health and Medical Research Fund.
Conflict of interest statement. None declared.

REFERENCES

1. Garneau,N.L., Wilusz,J. and Wilusz,C.J. (2007) The highways and byways of mRNA decay. *Nat. Rev. Mol. Cell Biol.*, **8**, 113–126.
2. He,F. and Jacobson,A. (2015) Nonsense-Mediated mRNA Decay: Degradation of defective transcripts is only part of the story. *Annu. Rev. Genet.*, **49**, 339–366.
3. Schmid,M. and Jensen,T.H. (2008) The exosome: a multipurpose RNA-decay machine. *Trends Biochem. Sci.*, **33**, 501–510.
4. Dziembowski,A., Lorentzen,E., Conti,E. and Seraphin,B. (2007) A single subunit, Dis3, is essentially responsible for yeast exosome core activity. *Nat. Struct. Mol. Biol.*, **14**, 15–22.
5. Schneider,C., Leung,E., Brown,J. and Tollervey,D. (2009) The N-terminal PIN domain of the exosome subunit Rrp44 harbors endonuclease activity and tethers Rrp44 to the yeast core exosome. *Nucleic Acids Res.*, **37**, 1127–1140.
6. Gudipati,R.K., Xu,Z., Lebreton,A., Seraphin,B., Steinmetz,L.M., Jacquier,A. and Libri,D. (2012) Extensive degradation of RNA precursors by the exosome in wild-type cells. *Mol. Cell*, **48**, 409–421.
7. Kadaba,S., Krueger,A., Trice,T., Krecic,A.M., Hinnebusch,A.G. and Anderson,J. (2004) Nuclear surveillance and degradation of hypomodified initiator tRNAMet in S. cerevisiae. *Genes Dev.*, **18**, 1227–1240.
8. Robinson,S.R., Oliver,A.W., Chevassut,T.J. and Newbury,S.F. (2015) The 3′ to 5′ Exoribonuclease DIS3: From structure and mechanisms to biological functions and role in human disease. *Biomolecules*, **5**, 1515–1539.
9. Mukherjee,D., Gao,M., O'Connor,J.P., Raijmakers,R., Pruijn,G., Lutz,C.S. and Wilusz,J. (2002) The mammalian exosome mediates the efficient degradation of mRNAs that contain AU-rich elements. *EMBO J.*, **21**, 165–174.
10. Bousquet-Antonelli,C., Presutti,C. and Tollervey,D. (2000) Identification of a regulated pathway for nuclear pre-mRNA turnover. *Cell*, **102**, 765–775.
11. Wyers,F., Rougemaille,M., Badis,G., Rousselle,J.C., Dufour,M.E., Boulay,J., Regnault,B., Devaux,F., Namane,A., Seraphin,B. *et al.* (2005) Cryptic pol II transcripts are degraded by a nuclear quality control pathway involving a new poly(A) polymerase. *Cell*, **121**, 725–737.
12. Park,S.H., Kukushkin,Y., Gupta,R., Chen,T., Konagai,A., Hipp,M.S., Hayer-Hartl,M. and Hartl,F.U. (2013) PolyQ proteins interfere with nuclear degradation of cytosolic proteins by sequestering the Sis1p chaperone. *Cell*, **154**, 134–145.
13. Gardner,R.G., Nelson,Z.W. and Gottschling,D.E. (2005) Degradation-mediated protein quality control in the nucleus. *Cell*, **120**, 803–815.
14. Heck,J.W., Cheung,S.K. and Hampton,R.Y. (2010) Cytoplasmic protein quality control degradation mediated by parallel actions of the E3 ubiquitin ligases Ubr1 and San1. *Proc. Natl. Acad. Sci. U.S.A.*, **107**, 1106–1111.
15. Prasad,R., Kawaguchi,S. and Ng,D.T. (2010) A nucleus-based quality control mechanism for cytosolic proteins. *Mol. Biol. Cell*, **21**, 2117–2127.
16. Park,S.H., Bolender,N., Eisele,F., Kostova,Z., Takeuchi,J., Coffino,P. and Wolf,D.H. (2007) The cytoplasmic Hsp70 chaperone machinery subjects misfolded and endoplasmic reticulum import-incompetent proteins to degradation via the ubiquitin-proteasome system. *Mol. Biol. Cell*, **18**, 153–165.
17. Gowda,N.K., Kandasamy,G., Froehlich,M.S., Dohmen,R.J. and Andreasson,C. (2013) Hsp70 nucleotide exchange factor Fes1 is essential for ubiquitin-dependent degradation of misfolded cytosolic proteins. *Proc. Natl. Acad. Sci. U.S.A.*, **110**, 5975–5980.
18. Kaganovich,D., Kopito,R. and Frydman,J. (2008) Misfolded proteins partition between two distinct quality control compartments. *Nature*, **454**, 1088–1095.
19. Miller,S.B., Ho,C.T., Winkler,J., Khokhrina,M., Neuner,A., Mohamed,M.Y., Guilbride,D.L., Richter,K., Lisby,M., Schiebel,E. *et al.* (2015) Compartment-specific aggregases direct distinct nuclear and cytoplasmic aggregate deposition. *EMBO J.*, **34**, 778–797.
20. Specht,S., Miller,S.B., Mogk,A. and Bukau,B. (2011) Hsp42 is required for sequestration of protein aggregates into deposition sites in Saccharomyces cerevisiae. *J. Cell Biol.*, **195**, 617–629.
21. Richter,K., Haslbeck,M. and Buchner,J. (2010) The heat shock response: life on the verge of death. *Mol. Cell*, **40**, 253–266.
22. Verghese,J., Abrams,J., Wang,Y. and Morano,K.A. (2012) Biology of the heat shock response and protein chaperones: budding yeast (Saccharomyces cerevisiae) as a model system. *Microbiol. Mol. Biol. Rev.*, **76**, 115–158.
23. Castells-Roca,L., Garcia-Martinez,J., Moreno,J., Herrero,E., Belli,G. and Perez-Ortin,J.E. (2011) Heat shock response in yeast involves changes in both transcription rates and mRNA stabilities. *PLoS One*, **6**, e17272.
24. Deka,K. and Saha,S. (2017) Arginylation: a new regulator of mRNA stability and heat stress response. *Cell Death Dis.*, **8**, e2604.
25. Petersen,R.B. and Lindquist,S. (1989) Regulation of HSP70 synthesis by messenger RNA degradation. *Cell Regul.*, **1**, 135–149.
26. Deka,K., Singh,A., Chakraborty,S., Mukhopadhyay,R. and Saha,S. (2016) Protein arginylation regulates cellular stress response by stabilizing HSP70 and HSP40 transcripts. *Cell Death Discov.*, **2**, 16074.
27. Chafekar,S.M. and Duennwald,M.L. (2012) Impaired heat shock response in cells expressing full-length polyglutamine-expanded huntingtin. *PLoS One*, **7**, e37929.
28. Bersuker,K., Hipp,M.S., Calamini,B., Morimoto,R.I. and Kopito,R.R. (2013) Heat shock response activation exacerbates inclusion body formation in a cellular model of Huntington disease. *J. Biol. Chem.*, **288**, 23633–23638.
29. Herbst,M. and Wanker,E.E. (2007) Small molecule inducers of heat-shock response reduce polyQ-mediated huntingtin aggregation. A possible therapeutic strategy. *Neurodegener Dis.*, **4**, 254–260.
30. Sittler,A., Lurz,R., Lueder,G., Priller,J., Lehrach,H., Hayer-Hartl,M.K., Hartl,F.U. and Wanker,E.E. (2001) Geldanamycin activates a heat shock response and inhibits huntingtin aggregation in a cell culture model of Huntington's disease. *Hum. Mol. Genet.*, **10**, 1307–1315.
31. Gietz,R.D. and Woods,R.A. (2002) Transformation of yeast by lithium acetate/single-stranded carrier DNA/polyethylene glycol method. *Methods Enzymol.*, **350**, 87–96.
32. Finger,A., Knop,M. and Wolf,D.H. (1993) Analysis of two mutated vacuolar proteins reveals a degradation pathway in the endoplasmic reticulum or a related compartment of yeast. *Eur. J. Biochem.*, **218**, 565–574.
33. Medicherla,B., Kostova,Z., Schaefer,A. and Wolf,D.H. (2004) A genomic screen identifies Dsk2p and Rad23p as essential components of ER-associated degradation. *EMBO Rep.*, **5**, 692–697.

34. Gupta,R., Kasturi,P., Bracher,A., Loew,C., Zheng,M., Villella,A., Garza,D., Hartl,F.U. and Raychaudhuri,S. (2011) Firefly luciferase mutants as sensors of proteome stress. *Nat. Methods*, **8**, 879–884.
35. Hiller,M.M., Finger,A., Schweiger,M. and Wolf,D.H. (1996) ER degradation of a misfolded luminal protein by the cytosolic ubiquitin-proteasome pathway. *Science*, **273**, 1725–1728.
36. Bengtson,M.H. and Joazeiro,C.A. (2010) Role of a ribosome-associated E3 ubiquitin ligase in protein quality control. *Nature*, **467**, 470–473.
37. Kong,K.Y., Tang,H.M., Pan,K., Huang,Z., Lee,T.H., Hinnebusch,A.G., Jin,D.Y. and Wong,C.M. (2014) Cotranscriptional recruitment of yeast TRAMP complex to intronic sequences promotes optimal pre-mRNA splicing. *Nucleic Acids Res.*, **42**, 643–660.
38. Wong,C.M., Tang,H.M., Kong,K.Y., Wong,G.W., Qiu,H., Jin,D.Y. and Hinnebusch,A.G. (2010) Yeast arginine methyltransferase Hmt1p regulates transcription elongation and termination by methylating Npl3p. *Nucleic Acids Res.*, **38**, 2217–2228.
39. Shiber,A., Breuer,W., Brandeis,M. and Ravid,T. (2013) Ubiquitin conjugation triggers misfolded protein sequestration into quality control foci when Hsp70 chaperone levels are limiting. *Mol. Biol. Cell*, **24**, 2076–2087.
40. Summers,D.W., Wolfe,K.J., Ren,H.Y. and Cyr,D.M. (2013) The Type II Hsp40 Sis1 cooperates with Hsp70 and the E3 ligase Ubr1 to promote degradation of terminally misfolded cytosolic protein. *PLoS One*, **8**, e52099.
41. Barreau,C., Paillard,L. and Osborne,H.B. (2005) AU-rich elements and associated factors: are there unifying principles? *Nucleic Acids Res.*, **33**, 7138–7150.
42. Aprile-Garcia,F., Tomar,P., Hummel,B., Khavaran,A. and Sawarkar,R. (2019) Nascent-protein ubiquitination is required for heat shock-induced gene downregulation in human cells. *Nat. Struct. Mol. Biol.*, **26**, 137–146.
43. Gong,Y., Kakihara,Y., Krogan,N., Greenblatt,J., Emili,A., Zhang,Z. and Houry,W.A. (2009) An atlas of chaperone-protein interactions in Saccharomyces cerevisiae: implications to protein folding pathways in the cell. *Mol. Syst. Biol.*, **5**, 275.
44. Adams,C.C. and Gross,D.S. (1991) The yeast heat shock response is induced by conversion of cells to spheroplasts and by potent transcriptional inhibitors. *J. Bacteriol.*, **173**, 7429–7435.
45. Calderwood,S.K., Murshid,A. and Prince,T. (2009) The shock of aging: molecular chaperones and the heat shock response in longevity and aging–a mini-review. *Gerontology*, **55**, 550–558.
46. Verbeke,P., Fonager,J., Clark,B.F. and Rattan,S.I. (2001) Heat shock response and ageing: mechanisms and applications. *Cell Biol. Int.*, **25**, 845–857.
47. Fang,N.N., Chan,G.T., Zhu,M., Comyn,S.A., Persaud,A., Deshaies,R.J., Rotin,D., Gsponer,J. and Mayor,T. (2014) Rsp5/Nedd4 is the main ubiquitin ligase that targets cytosolic misfolded proteins following heat stress. *Nat. Cell Biol.*, **16**, 1227–1237.
48. Gupta,R., Kus,B., Fladd,C., Wasmuth,J., Tonikian,R., Sidhu,S., Krogan,N.J., Parkinson,J. and Rotin,D. (2007) Ubiquitination screen using protein microarrays for comprehensive identification of Rsp5 substrates in yeast. *Mol. Syst. Biol.*, **3**, 116.
49. Meriin,A.B., Zhang,X., Miliaras,N.B., Kazantsev,A., Chernoff,Y.O., McCaffery,J.M., Wendland,B. and Sherman,M.Y. (2003) Aggregation of expanded polyglutamine domain in yeast leads to defects in endocytosis. *Mol. Cell Biol.*, **23**, 7554–7565.
50. Astuti,D., Morris,M.R., Cooper,W.N., Staals,R.H., Wake,N.C., Fews,G.A., Gill,H., Gentle,D., Shuib,S., Ricketts,C.J. *et al.* (2012) Germline mutations in DIS3L2 cause the Perlman syndrome of overgrowth and Wilms tumor susceptibility. *Nat. Genet.*, **44**, 277–284.
51. Tomecki,R., Kristiansen,M.S., Lykke-Andersen,S., Chlebowski,A., Larsen,K.M., Szczesny,R.J., Drazkowska,K., Pastula,A., Andersen,J.S., Stepien,P.P. *et al.* (2010) The human core exosome interacts with differentially localized processive RNases: hDIS3 and hDIS3L. *EMBO J.*, **29**, 2342–2357.
52. Ustianenko,D., Hrossova,D., Potesil,D., Chalupnikova,K., Hrazdilova,K., Pachernik,J., Cetkovska,K., Uldrijan,S., Zdrahal,Z. and Vanacova,S. (2013) Mammalian DIS3L2 exoribonuclease targets the uridylated precursors of let-7 miRNAs. *RNA*, **19**, 1632–1638.